iScience

CellPress
OPEN ACCESS

Article

Site-specific phosphorylation of ZYG-1 regulates ZYG-1 stability and centrosome number

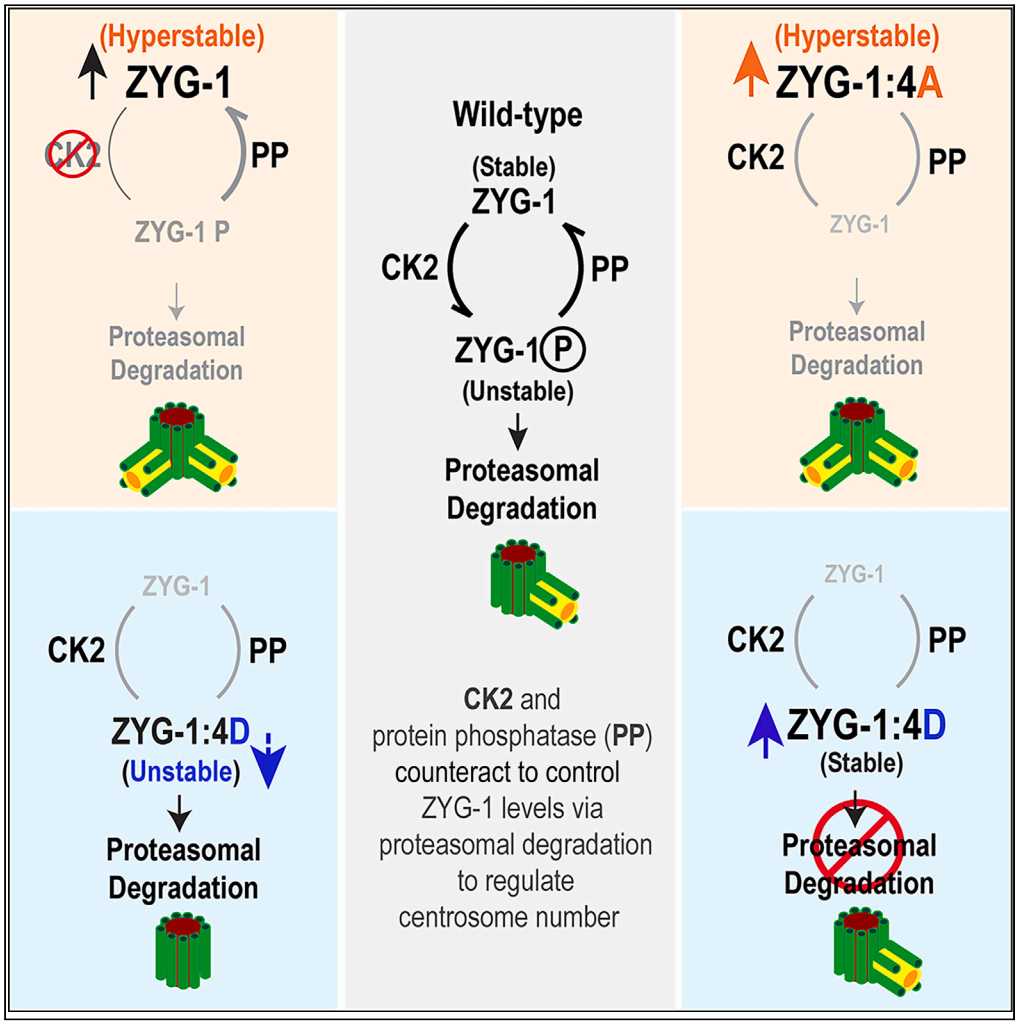

Jeffrey C. Medley, Rachel N. Yim, Joseph DiPanni, ..., Colin Wu, Megan Kabara, Mi Hye Song

msong2@oakland.edu

Highlights

Depleting casein kinase II (CK2) leads to extra centrosomes

CK2 directly phosphorylates ZYG-1

ZYG-1 phosphorylation by CK2 triggers proteasomal degradation of ZYG-1

CK2-dependent phosphorylation of ZYG-1 regulates centrosome number

Medley et al., iScience *26*, 108410
December 15, 2023
https://doi.org/10.1016/j.isci.2023.108410

iScience

CellPress
OPEN ACCESS

Article

Site-specific phosphorylation of ZYG-1 regulates ZYG-1 stability and centrosome number

Jeffrey C. Medley,[1] Rachel N. Yim,[1] Joseph DiPanni,[1] Brandon Sebou,[1] Blake Shaffou,[1] Evan Cramer,[2] Colin Wu,[2] Megan Kabara,[1,3] and Mi Hye Song[1,4,*]

SUMMARY

Spindle bipolarity is critical for genomic integrity. As centrosome number often dictates bipolarity, tight control of centrosome assembly is vital for faithful cell division. The master centrosome regulator ZYG-1/Plk4 plays a pivotal role in this process. In *C. elegans*, casein kinase II (CK2) negatively regulates centrosome duplication by controlling centrosome-associated ZYG-1 levels. Here, we investigated CK2 as a regulator of ZYG-1 and its impact on centrosome assembly. We show that CK2 phosphorylates ZYG-1 *in vitro* and physically interacts with ZYG-1 *in vivo*. Depleting CK2 or blocking ZYG-1 phosphorylation at CK2 target sites leads to centrosome amplification. Non-phosphorylatable ZYG-1 mutants exhibit elevated ZYG-1 levels, leading to increased ZYG-1 and downstream factors at centrosomes, thus driving centrosome amplification. Moreover, inhibiting the 26S proteasome prevents degradation of the phospho-mimetic ZYG-1. Our findings suggest that CK2-dependent phosphorylation of ZYG-1 controls ZYG-1 levels via proteasomal degradation to limit centrosome number.

INTRODUCTION

During cell division, equal distribution of chromosomes into each daughter cell is essential to maintain genomic integrity. As microtubule-organizing centers, centrosomes are critical for establishing mitotic bipolar spindles that ensure accurate transmission of genomic content.[1] Errors in centrosome number disrupt spindle bipolarity, leading to chromosome missegregation, and aberrant centrosomes are linked with human cancers and developmental defects.[2,3] To maintain proper centrosome numbers, centrosomes must duplicate only once per cell cycle through a process tightly regulated and coupled with the cell cycle.[1,4]

Protein phosphorylation has emerged as a critical mechanism that controls the activity and abundance of key centrosome proteins.[5] In humans, the kinase Plk4 is a master regulator of centrosome biogenesis.[6] Plk4 phosphorylates the C-terminal STAN domain of STIL/Ana2/SAS-5, facilitating the direct binding of STIL/Ana2 to SAS-6 and initiating the procentriole formation.[7–10] In a subsequent step, Plk4 phosphorylates another site (S428) of STIL, promoting STIL binding to CPAP/SAS-4.[11] The *C. elegans* ZYG-1, the human Plk4-related kinase, is critical for centrosome duplication.[12] ZYG-1 localizes to the site of procentriole formation[13] and is necessary for centrosomal recruitment of SAS-5 and SAS-6.[14–16] ZYG-1, independently of its kinase activity, directly binds to SAS-6 to recruit SAS-6 and SAS-5 to nascent centrioles, whereas stable incorporation of SAS-6 into centrioles requires kinase activity of ZYG-1 through an unknown mechanism.[17]

The abundance of centrosome regulators is critical for centrosome number in centrosome assembly. Autophosphorylation and subsequent proteasomal degradation through the SCF-βTrCP/Slimb E3 ubiquitin ligase-dependent pathway have been identified as mechanisms controlling the levels of human Plk4.[18,19] This regulatory mechanism appears to be evolutionarily conserved, involving the SCF-Slimb/βTrCP E3 ubiquitin ligase and the Slimb/βTrCP-binding motif (SBM) in *C. elegans*, *Drosophila*, and human cells.[19–22] In *Drosophila* and human cells, autophosphorylation of the SBM triggers $SCF^{Slimb/\beta TrCP}$ binding to Plk4, promoting Plk4 degradation.[18,23,24] However, it remains elusive whether autophosphorylation of ZYG-1 *in C. elegans* has a similar role in $SCF^{Slimb/\beta TrCP}$-mediated degradation of ZYG-1. Several *C. elegans* genes have been identified that modulate ZYG-1 activity in centrosome assembly through multiple regulatory mechanisms, including transcription, RNA binding, proteolysis, and protein phosphorylation.[25–29] Studies in *C. elegans* have shown that protein phosphorylation influences cellular and centrosomal levels of ZYG-1, which is critical for normal centrosome number and microtubule-nucleating activity.[25,29–31] $PP2A^{SUR-6/B55}$ exhibits a strong genetic interaction with ZYG-1 and SAS-5, and $PP2A^{SUR-6/B55}$-dependent dephosphorylation appears to stabilize ZYG-1 and SAS-5 by protecting them from proteasomal destruction.[31] It remains unknown what kinase counteracts $PP2A^{SUR-6/B55}$-mediated dephosphorylation of these centrosome proteins in *C. elegans*, whereas PP2A-dependent dephosphorylation has been proposed to counteract Plk4 autophosphorylation and stabilizes Plk4 in humans and flies.[32]

[1]Department of Biological Sciences, Oakland University, Rochester, MI, USA
[2]Department of Chemistry, Oakland University, Rochester, MI, USA
[3]University of Connecticut School of Medicine, Office of Graduate Medical Education, Farmington, CT, USA
[4]Lead contact
*Correspondence: msong2@oakland.edu
https://doi.org/10.1016/j.isci.2023.108410

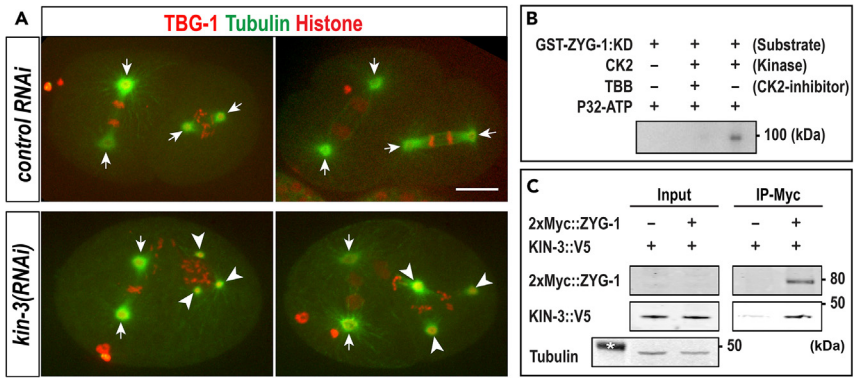

Figure 1. Loss of CK2 leads to extra centrosomes

(A) Still images of embryos expressing GFP::β-tubulin, mCherry::TBG-1 (γ-tubulin), and mCherry::histone at the second mitosis. Arrows indicate bipolar spindles, and arrowheads mark tripolar mitotic spindles. Bar: 10 μm.

(B) Autoradiogram of GST-ZYG-1 (kinase-dead: KD) incubated with CK2.

(C) 2xMyc::ZYG-1 co-precipitates with KIN-3::V5. ~5% of lysates were loaded in input. * marks a position of ~50 kDa molecular weight.

In *C. elegans*, casein kinase II (CK2) has been shown to negatively regulate centrosome duplication.[25] CK2 is a tetrameric holoenzyme comprising two catalytic (CK2α) and two regulatory (CK2β) subunits. The *C. elegans* genome contains the *kin-3* and *kin-10* genes that encode for the CK2α and CK2β subunits, respectively,[33,34] and CK2 functions in various cellular processes[35–43] including cell division.[25] CK2 is an evolutionarily conserved serine/threonine protein kinase that targets over 500 substrates.[44,45] In human cells, CK2 activity is elevated in both tumor cells and normal proliferating cells,[46,47] and deregulated CK2α activity leads to centrosome amplification, although the precise mechanism.[48]

In *C. elegans*, CK2 negatively regulates centrosome duplication by controlling centrosome-associated ZYG-1 levels.[25] However, the specific substrate(s) of CK2 and phosphorylation sites involved in centrosome assembly have not yet been identified. In this study, we investigated ZYG-1 as a potential substrate of CK2 and examined the functional impact of site-specific phosphorylation of ZYG-1 on centrosome assembly *in vivo*. Blocking phosphorylation of ZYG-1 at potential CK2 target sites phenocopies loss of CK2 in centrosome assembly. Non-phosphorylatable (NP) ZYG-1 is protected from degradation, promoting centrosome amplification. Our findings suggest that multi-site phosphorylation of ZYG-1, likely by CK2, regulates ZYG-1 stability and is critical for the proper centrosome number in *C. elegans* embryos.

RESULTS

Loss of CK2 results in extra centrosomes

It has been shown that *kin-3(RNAi)*-mediated partial knockdown of KIN-3, the catalytic subunit of CK2, does not significantly impact embryonic development.[25,42] By contrast, embryos further depleted of KIN-3, when animals were treated with *kin-3(RNAi)* for extended hours (40–48 h), were partially inviable with various cell division phenotypes.[25] Remarkably, in these conditions, we observed the formation of tripolar spindles reproducibly, albeit infrequently (<3%) (Figures 1A and S1A). In *C. elegans*, sperm provides a pair of centrioles to the embryo during fertilization. During the first mitosis, the paternal centriole pair segregates and duplicates, then two centrosomes establish bipolar spindles. Live imaging shows that *kin-3(RNAi)*-treated embryos undergo normal cytokinesis at the first mitosis but form tripolar spindles at the second mitosis (Figure S1A), suggesting that extra centrosomes likely arise from centrosome overduplication. These observations illustrate that inhibiting CK2 kinase activity leads to centrosome amplification in *C. elegans* embryos, indicating that CK2 kinase activity is critical for the integrity of centrosome number, potentially through phosphorylation of one or more centrosome proteins.

CK2 phosphorylates ZYG-1 *in vitro*

While CK2 kinase activity influences centrosome assembly in *C. elegans* embryos,[25] we do not know the specific substrate(s) and sites phosphorylated by CK2 critical for centrosome assembly. A compelling candidate is the kinase ZYG-1, a master regulator of centrosome duplication.[12] In *C. elegans*, increased centrosomal ZYG-1 or overexpressing ZYG-1 leads to extra centrosomes in early embryos[20,29] and seam cells.[49] Because CK2 kinase activity negatively regulates centrosome duplication by controlling ZYG-1 levels at centrosomes,[25] we hypothesized CK2 directly phosphorylates ZYG-1, and that the phosphorylation state of ZYG-1 influences ZYG-1 activity in regulating centrosome assembly. In this study, we use the term "ZYG-1 activity" to denote the overall ZYG-1 function essential for centrosome assembly, including both its kinase-dependent and kinase-independent roles. We first tested whether human recombinant CK2 can phosphorylate ZYG-1 *in vitro* (Figure 1B). Since the *C. elegans* kinase ZYG-1 is shown to be autophosphorylated *in vitro*,[12] we used the kinase-dead ZYG-1 (KD-ZYG-1^{K41M};[12]) as a substrate to eliminate auto-phosphorylated ZYG-1 for *in vitro* kinase assay. Autoradiograph illustrates that CK2 phosphorylates KD-ZYG-1^{K41M}, and this phosphorylation was blocked by a CK2 kinase inhibitor (TBB). Furthermore, our immunoprecipitation (IP) assays using embryonic lysates suggest a physical interaction between 2xMyc::ZYG-1 and KIN-3::V5 *in vivo*[20,50] (Figure 1C). These results support our hypothesis that CK2 directly phosphorylates ZYG-1.

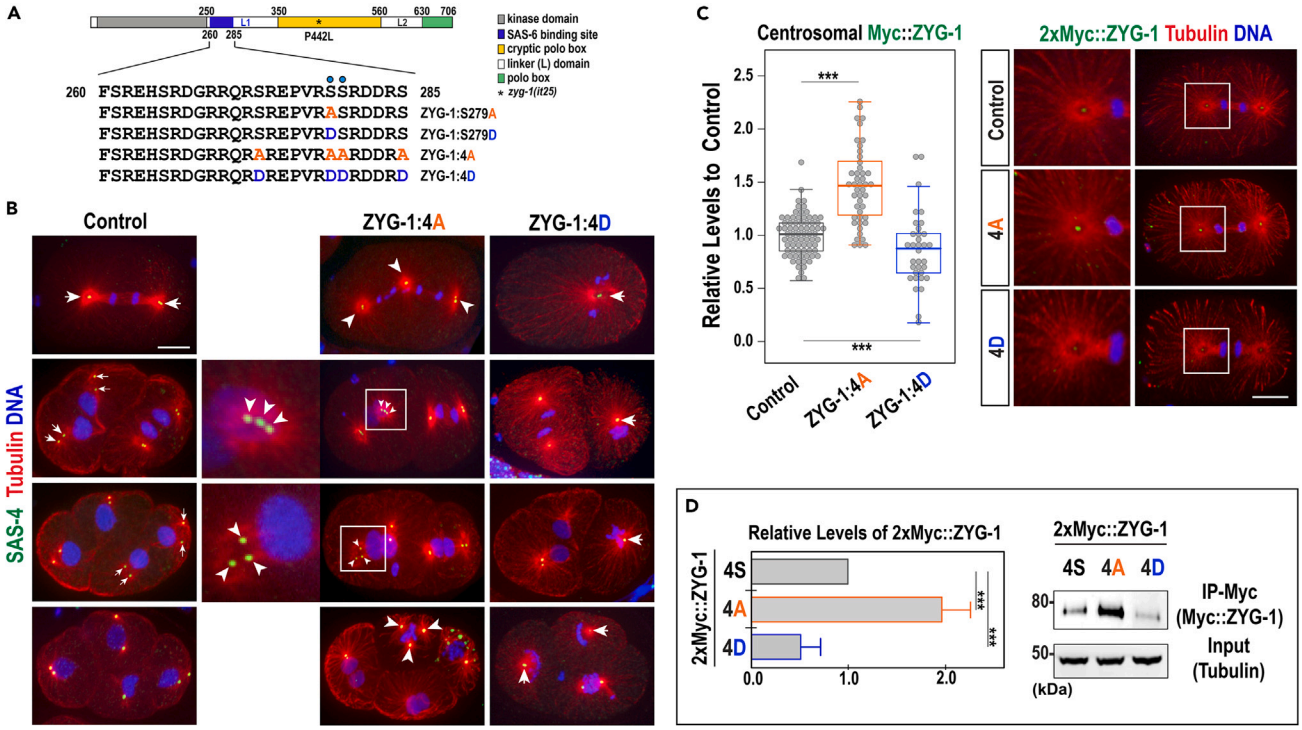

Figure 2. The phosphorylation state of ZYG-1 regulates centrosome number and ZYG-1 stability

(A) ZYG-1 protein structure illustrates locations of functional domains, including kinase domain (gray), SAS-6-binding region (blue), cryptic polo box (CPB: yellow), polo box (green), and two linker (L1 and L2) domains (white). * indicating the *zyg-1(it25)* mutation (P442L) within the CPB domain. Blue dots indicate S279 and S280. The sites of our phospho-mutants (S279A, S279D, 4A, and 4D) are depicted.

(B) Immunostained embryos display abnormal centrosome numbers in ZYG-1 phospho-mutants. Tripolar spindles are observed in ZYG-1:4A and 2xMyc::ZYG-1:4A mutants and monopolar spindles in ZYG-1:4D and 2xMyc::ZYG-1:4D mutants. For ZYG-1:4A and 2xMyc::ZYG-1:4A mutants, insets highlight centrosomes with three centriolar foci stained with SAS-4 at the second telophase.

(C) (Left) Quantification of centrosomal 2xMyc::ZYG-1 levels during the first anaphase. Each dot represents a centrosome. In the plot, box ranges from the first through third quartile of the data. Thick bar indicates the median. Lines extend to the minimum and maximum data point excluding outliers defined as beyond 1.5 times the interquartile range. (Right) Immunostained embryos.

(D) (Left) Relative levels of total 2xMyc::ZYG-1 in Myc-pulldown normalized against Tubulin in input (mean ± SD). (Right) Myc-IP of 2xMyc::ZYG-1 embryonic lysates. ~5% of total lysates were loaded in input. (B and C) Insets magnified 4-fold. Bar: 10 μm. (C and D) ***$p < 0.001$ (two-tailed unpaired *t* tests).

CK2 consensus sites in the L1 domain of ZYG-1

CK2 is a serine/threonine protein kinase that favors substrates containing acidic residues downstream of the phosphorylation sites (S/TxxD/E).[51,52] Using *in silico* approaches (KinasePhos3.0[53] and GPS 5.0[54]), we predicted potential phosphorylation sites in ZYG-1, identifying S279, S280, S620, and T621 as having the highest likelihood of CK2 consensus motifs (Table S1). These potential CK2 target sites are located in two distinct regions outside the kinase domain: S279/S280 in the Linker 1 (L1) domain and S620/T621 in the Linker 2 (L2) domain (Figure 2A). The sequence alignments illustrate that S279 and S280 exhibit strong evolutionary conservation (Figure S2A), but S620 and T621 have weaker conservation (Figure S2B) within the *Caenorhabditis* genus. Considering sequence conservation, we focused on S279 and neighboring serine residues within the L1 domain that is critical for ZYG-1 function in centrosome assembly.[17,20] S279 is part of a serine cluster (aa260-285: Figure 2A) conforming to the minimal CK2 consensus motif and highly conserved throughout the *Caenorhabditis* genus (Figure S2A). Given that the *C. elegans* ZYG-1 is evolutionarily divergent from Plk4 orthologs, S279 and adjacent serine sites do not appear to be conserved in the human Plk4. However, Plk4 contains several serine/threonine residues that conform to the CK2 consensus motif (Table S2). Intriguingly, this ZYG-1 region (aa260-280) coincides with the direct binding domain of ZYG-1 to SAS-6,[17] highlighting the functional significance of this ZYG-1 region in centrosome duplication. Herein, we will refer to this region as ZYG-1:4S.

To test whether CK2 phosphorylates ZYG-1 at these sites, we performed *in vitro* kinase assay using human recombinant CK2 and the ZYG-1 peptides (aa269-289) containing four serine residues as a substrate (Figure S2C). Autoradiogram of thin-layer chromatography (TLC) revealed that CK2 phosphorylates the wild-type ZYG-1 peptide but not the ZYG-1:4A peptide where four sites (S273, S279, S280, and S285) were replaced with alanine. By contrast, the CK2 inhibitor TBB reduced CK2-dependent phosphorylation of the ZYG-1 peptide. Mass spectrometry analysis of *in vitro* kinase reactions using the ZYG-1 peptide substrate and CK2 confirmed the reproducible phosphorylation of at least one serine residue (S279 or S280) within this ZYG-1 peptide (Figure S2D[55]). Our data suggest CK2 directly phosphorylates at least one serine residue in the ZYG-1 L1 domain.

Table 1. Genetic analysis

Strain	°C	% Embryonic Viability (ave ±s.d.)	n (progeny)
wild-type (N2)		100 ± 0	1803
ZYG-1^{S279A}		98.7 ± 2.5	1542
ZYG-1^{4A}		90.4 ± 5.0	2052
ZYG-1^{S279D}		99.0 ± 3.3	1669
ZYG-1^{4D}		98.6 ± 1.7	1718
zyg-1(it25)	22.5	8.8 ± 8.2	1275
ZYG-1^{S279A}: *zyg-1(it25)*		31.1 ± 19.9	1301
ZYG-1^{4A}: *zyg-1(it25)*		96.1 ± 3.6	3426
ZYG-1^{S279D}: *zyg-1(it25)*		2.5 ± 2.8	1401
ZYG-1^{4D}: *zyg-1(it25)*		1.9 ± 3.4	1529
wild-type (N2)		100 ± 0	400
ZYG-1^{S279A}		100 ± 0	504
ZYG-1^{4A}		87.7 ± 6.4	457
ZYG-1^{S279D}		97.6 ± 1.2	573
ZYG-1^{4D}		99.1 ± 0.6	336
zyg-1(it25)	23.0	0.3 ± 0.7	716
ZYG-1^{S279A}: *zyg-1(it25)*		3.7 ± 3.1	301
ZYG-1^{4A}: *zyg-1(it25)*		19.7 ± 6.2	514
ZYG-1^{S279D}: *zyg-1(it25)*		0 ± 0	239
ZYG-1^{4D}: *zyg-1(it25)*		0 ± 0	494

Non-phosphorylatable ZYG-1 mutation leads to centrosome amplification

To address the functional impacts of site-specific phosphorylation of ZYG-1 *in vivo*, we used CRISPR/Cas9 editing to mutate S279 to a NP alanine, termed ZYG-1^{S279A} and a phospho-mimetic (PM) aspartate, termed ZYG-1^{S279D} at the endogenous locus (Figure 2A). In parallel, we simultaneously mutated four serine residues (S273, S279, S280, and S285; Table S1) to alanine, termed ZYG-1,^{4A} or aspartate, termed ZYG-1.^{4D} The homozygous ZYG-1 phospho-mutants we generated were mostly viable, with ZYG-1^{4A} mutants producing a low rate of embryonic lethality (Table 1). Since *kin-3(RNAi)*-mediated inhibition of CK2 leads to tripolar spindle formation (Figure 1A), we speculated that mutating a subset of CK2 target sites to NP alanine (NP-ZYG-1 mutations) should partially phenocopy loss of CK2, including extra centrosomes. We first observed centrosome behavior to determine how the phosphorylation state of ZYG-1 affected centrosome duplication (Figures 2B, S1B, and S3). Intriguingly, we detected extra centrosomes in ZYG-1^{4A} and 2xMyc::ZYG-1^{4A} mutant embryos (<10% and ~30%, respectively, n > 100; see Figure S3D for additional strain information), starting at the first mitosis and later cell divisions. Extra centrosomes resemble phenotypes arising from Plk4 overexpression,[6] implying that the ZYG-1^{4A} mutation upregulates ZYG-1 activity leading to centrosome amplification. Furthermore, we observed various cell division phenotypes in ZYG-1^{4A} mutant embryos (Figure S3A), including DNA mis-segregation, cytokinesis failure, detached centrosomes, and expanded PCM morphology, similar to phenotypes observed in embryos depleted of CK2.[25] These results show that the NP-ZYG-1^{4A} mutation phenocopies loss of CK2 during *C. elegans* embryogenesis. In contrast, the ZYG-1^{4D} and 2xMyc::ZYG-1^{4D} mutation caused monopolar spindle formation in one-cell and later-stage embryos (<10% and ~30%, respectively, n > 100) (Figures 2B and S3B, see Figure S3D for additional strain information), indicating that the PM-ZYG-1^{4D} mutation down-regulates ZYG-1 activity and impairs centrosome duplication during spermatogenesis and mitotic divisions. Compared to ZYG-1^{4A} and ZYG-1^{4D} mutants, mutating a single site at S279 reduced the extent of these phenotypes. ZYG-1^{S279A} mutants displayed similar yet less pronounced phenotypes (Figure S3C) than ZYG-1^{4A} mutants, while ZYG-1^{S279D} mutants did not manifest apparent phenotypes. Together, these observations suggest that ZYG-1 phosphorylation at multiple sites is critical for centrosome duplication in early embryonic cell division.

Non-phosphorylatable ZYG-1 leads to elevated ZYG-1 levels

As a previous study showed that *kin-3(RNAi)* (1.7 ± 0.7-fold) or chemical inhibition of CK2 kinase activity (1.48 ± 0.57-fold) leads to elevated centrosomal ZYG-1,[25] we examined how the NP-and PM-ZYG-1 mutations affected ZYG-1 levels at centrosomes. To facilitate this assay, we introduced an N-terminal 2xMyc tag at the endogenous *zyg-1* locus by CRISPR/Cas9 editing.[20] By immunostaining embryos with anti-Myc, we quantified the fluorescence intensity of centrosome-associated 2xMyc::ZYG-1 during the first anaphase (Figure 2C). The NP-ZYG-1^{4A} still localizes to centrosomes, indicating alanine replacements at these serine sites did not impair ZYG-1 loading to centrosomes. Quantitative immunofluorescence (IF) revealed that ZYG-1^{4A} mutant embryos exhibit significantly increased 2xMyc::ZYG-1 signals at centrosomes (1.47 ± 0.45-fold, $p < 0.001$), while ZYG-1^{4D} mutants showed decreased levels (0.81 ± 0.28-fold, $p < 0.01$), compared to wild-type controls

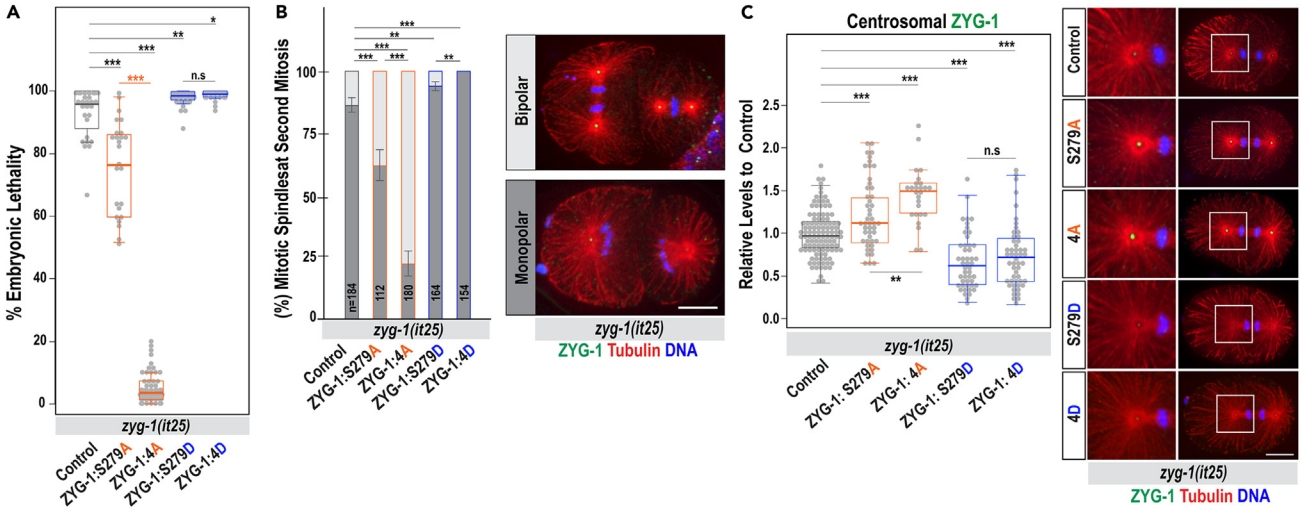

Figure 3. Multi-site phosphorylation of ZYG-1 regulates ZYG-1 activity and centrosome duplication

(A) Embryonic viability at 22.5°C (Table 1). Each dot represents a hermaphrodite.

(B) (Left) Quantification of mitotic spindles at the second mitosis at 23°C (mean ± SD). n is the number of blastomeres. (Right) Immunostained embryos undergoing second mitosis illustrate monopolar (dark gray) or bipolar (light gray) spindles.

(C) (Left) Quantification of centrosomal ZYG-1 levels at the first anaphase. Each dot represents a centrosome. (Right) Embryos stained for ZYG-1 at the first anaphase. Insets magnified 4-fold. (A and C) Boxes range from the first through third quartile of the data. Thick bar indicates the median. Lines extend to the minimum and maximum data point excluding outliers defined as beyond 1.5 times the interquartile range. (B and C) Bar: 10 μm. (A–C) n.s $p > 0.05$, *$p < 0.05$, **$p < 0.01$, ***$p < 0.001$ (two-tailed unpaired *t* tests).

(1.00 ± 0.20-fold). Similar trends were observed at the first metaphase (Figure S4A). Our data illustrate that the phosphorylation state of ZYG-1 affects its protein levels at centrosomes.

Increased levels of cellular ZYG-1 may account for elevated centrosomal ZYG-1 in NP-ZYG-1 mutants. Following Myc-pulldown using embryonic lysates expressing 2xMyc::ZYG-1, we could detect Myc-tagged ZYG-1, with significantly increased levels (1.98 ± 0.51-fold, $p < 0.0001$, $n = 6$) of 2xMyc::ZYG-1 in ZYG-1^{4A} embryos, and reduced levels (0.51 ± 0.19-fold, $p < 0.0001$, $n = 6$) in ZYG-1^{4D} embryos (Figure 2D). Our quantitative immunoblot supports a model where NP-ZYG-1 is hyperstabilized, leading to increased levels of cellular ZYG-1, thereby more ZYG-1 loaded to centrosomes.

Non-phosphorylatable ZYG-1 restores centrosome duplication in *zyg-1(it25)*

Depleting CK2 restores centrosome duplication and embryonic viability to hypomorphic *zyg-1(it25)* mutants.[25] The *zyg-1(it25)* mutation causes a single amino acid substitution (P442L) in the cryptic polo box (CPB) domain critical for centrosomal targeting of ZYG-1 (Figure 2A).[56] We asked if the NP-ZYG-1 mutation, mimicking loss of CK2, could produce similar effects on *zyg-1(it25)* mutants. In this scenario, the NP-ZYG-1 mutation should restore embryonic viability and centrosome duplication to *zyg-1(it25)* mutants. To test this, we used CRISPR/Cas9 editing and introduced equivalent phospho-mutations to *zyg-1(it25)* mutants at the endogenous locus. In the temperature-sensitive *zyg-1(it25)* mutant embryos grown at the restrictive temperature 24°C, centrosome duplication fails during the first cell cycle, resulting in monopolar spindles at the second mitosis and 100% embryonic lethality.[12] Given the fact that CK2 depletion does not restore embryonic viability to *zyg-1(it25)* mutants at the restrictive temperature[25] (24°C), we used the semi-restrictive temperature conditions (22.5°C or 23°C) where the hypomorphic ZYG-1 function in *zyg-1(it25)* mutants remain partially active. Remarkably, the ZYG-1^{4A} mutation led to a significant restoration (>10-fold) of embryonic viability (96.1 ± 3.6%), and the ZYG-1^{S279A} mutation produced a relatively moderate but significant restoration (31.1 ± 19.9%, 3.5-fold) to *zyg-1(it25)* mutants (8.8 ± 8.2%) at 22.5°C (Table 1; Figure 3A). By contrast, the ZYG-1^{4D} and ZYG-1^{S279D} mutations produced opposite effects on *zyg-1(it25)* mutants (Table 1; Figure 3A). Similar trends were observed at 23°C (Table 1). These results suggest that the NP-ZYG-1 mutation upregulates ZYG-1 activity, compensating for the hypomorphic ZYG-1 function in *zyg-1(it25)* mutants, while the PM-ZYG-1 mutations have the opposite effect.

Given that ZYG-1 is essential for centrosome duplication, restoring embryonic viability to *zyg-1(it25)* mutants likely results from successful centrosome duplication. To examine how ZYG-1 phospho-mutations affected centrosome duplication in the *zyg-1(it25)* mutant, we scored for bipolar spindle formation during the second mitosis (Figure 3B). Consistent with the genetic suppression, both NP-ZYG-1^{S279A} and ZYG-1^{4A} mutations restored bipolar spindles to *zyg-1(it25)* mutants (13.8 ± 6.2%), with the ZYG-1^{4A} mutation (77.7 ± 10%) exhibiting a higher rate of bipolar spindles than the ZYG-1^{S279A} mutation (38.1 ± 12%). Conversely, both PM-ZYG-1 mutations (ZYG-1^{S279D} and ZYG-1^{4D}) decreased bipolar spindle formation (6 ± 3.6% and 0%, respectively). Similar to loss of CK2, the NP-ZYG-1 mutations appear to enhance ZYG-1 activity, thereby restoring centrosome duplication and embryonic viability to *zyg-1(it25)* mutants, while the PM-ZYG-1 mutations diminish ZYG-1 activity and aggravate *zyg-1(it25)* phenotypes.

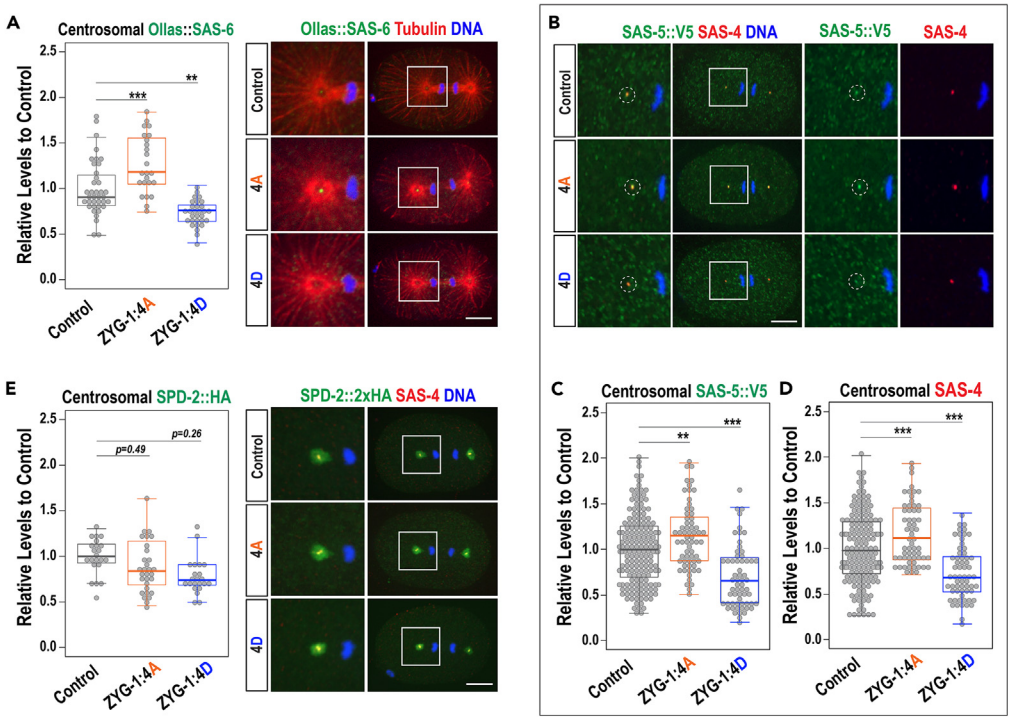

Figure 4. The phosphorylation state of ZYG-1 influences centrosomal levels of downstream factors

ZYG-1 phospho-mutant embryos stained for (A) Ollas::SAS-6, (B) SAS-5::V5 and SAS-4, (E) SPD-2::2xHA. (B) The dotted circles highlight co-localization of SAS-5::V5 and SAS-4. (A, B, and E) Insets magnified 4-fold. Bar: 10 μm. (A, C–E) Plots show quantification of centrosomal proteins at the first mitotic anaphase. Boxes range from the first through third quartile of the data. Thick bar indicates the median. Lines extend to the minimum and maximum data point excluding outliers defined as beyond 1.5 times the interquartile range. **p < 0.01, ***p < 0.001 (two-tailed unpaired *t* tests).

Increased levels of centrosomal ZYG-1 in ZYG-1^{4A} mutants may explain suppression of *zyg-1(it25)* phenotypes by the NP-ZYG-1 mutation. To directly test this, we compared centrosomal ZYG-1 levels in *zyg-1(it25)* mutant backgrounds (Figure 3C). Quantitative IF using anti-ZYG-1[57] illustrate significantly increased levels of centrosomal ZYG-1 in ZYG-1^{4A}: *zyg-1(it25)* (1.45 ± 0.33-fold, p < 0.001) and ZYG-1^{S279A}: *zyg-1(it25)* (1.26 ± 0.43-fold, p < 0.001) embryos, compared to *zyg-1(it25)* controls (1.00 ± 0.26-fold) during the first anaphase. Notably, the ZYG-1^{4A} mutation produced a stronger impact on centrosomal ZYG-1 levels than the ZYG-1^{S279A} mutation, consistent with more robust *zyg-1* suppression by ZYG-1^{4A} than the ZYG-1^{S279A} mutation (Figures 3A and 3B; Table1). Conversely, reduced centrosomal ZYG-1 levels were observed in the ZYG-1^{4D}: *zyg-1(it25)* (0.75 ± 0.42-fold, p < 0.001) and ZYG-1^{S279D}: *zyg-1(it25)* (0.67 ± 0.33-fold, p < 0.001) mutants at the first anaphase. Together, our results suggest that phosphorylation of ZYG-1 at multi-sites regulates centrosomal ZYG-1 levels, thereby influencing ZYG-1 activity in centrosome assembly.

ZYG-1 phosphorylation affects centrosomal loading of downstream centrosome factors

In the molecular hierarchy of centrosome assembly, SPD-2 acts upstream and promotes centrosomal targeting of ZYG-1 via direct electrostatic interaction,[56] and ZYG-1 is required for centrosomal recruitment of downstream centrosome factors, SAS-6, SAS-5, and SAS-4.[14,17] Then, elevated centrosomal ZYG-1 in ZYG-1^{4A} mutants may enhance centrosomal recruitment of downstream factors, leading to centrosome amplification. Alternatively, the phosphorylation state of ZYG-1 could affect its interaction with other centrosome factors positively or negatively.

Quantitative IF during the first anaphase reveals that NP-ZYG-1^{4A} mutant embryos exhibit increased levels of centrosomal SAS-6 (1.26 ± 0.31-fold, p < 0.001), whereas ZYG-1^{4D} mutant embryos show reduced SAS-6 levels (0.73 ± 0.17-fold, p < 0.01), compared to wild-type controls (1.00 ± 0.28-fold) (Figure 4A). Increased SAS-6 levels in NP-ZYG-1^{4A} mutant centrosomes might result from elevated centrosomal ZYG-1. Alternatively, the phosphorylation state of ZYG-1 could affect the ZYG-1-SAS-6 binding affinity through charge changes, as the phosphorylation cluster (ZYG-1:4S) coincides with the ZYG-1 domain that directly interacts with SAS-6 through electrostatic attraction.[17] To address the latter, we performed quantitative immunoblot analysis following Myc-IP to compare the relative levels of SAS-6 associated with 2xMyc::ZYG-1 (Figure S2E). Both Myc-IP of ZYG-1^{4A} and ZYG-1^{4D} mutants show a higher ratio of SAS-6 to 2xMyc::ZYG-1 than controls, indicating that charge differences between two mutants do not explain the opposing effects on centrosomal SAS-6 levels. Thus, elevated centrosomal ZYG-1 in ZYG-1^{4A} mutants seems more likely to further enhance SAS-6 recruitment to centrosomes.

ZYG-1 is also required for centrosomal SAS-5 loading, and SAS-5 and SAS-6 are co-dependent for centrosomal localization.[15] Consistent with SAS-6, we observed significantly increased SAS-5 in ZYG-1^{4A} mutant centrosomes (1.20 ± 0.43-fold, p < 0.001), but decreased levels in

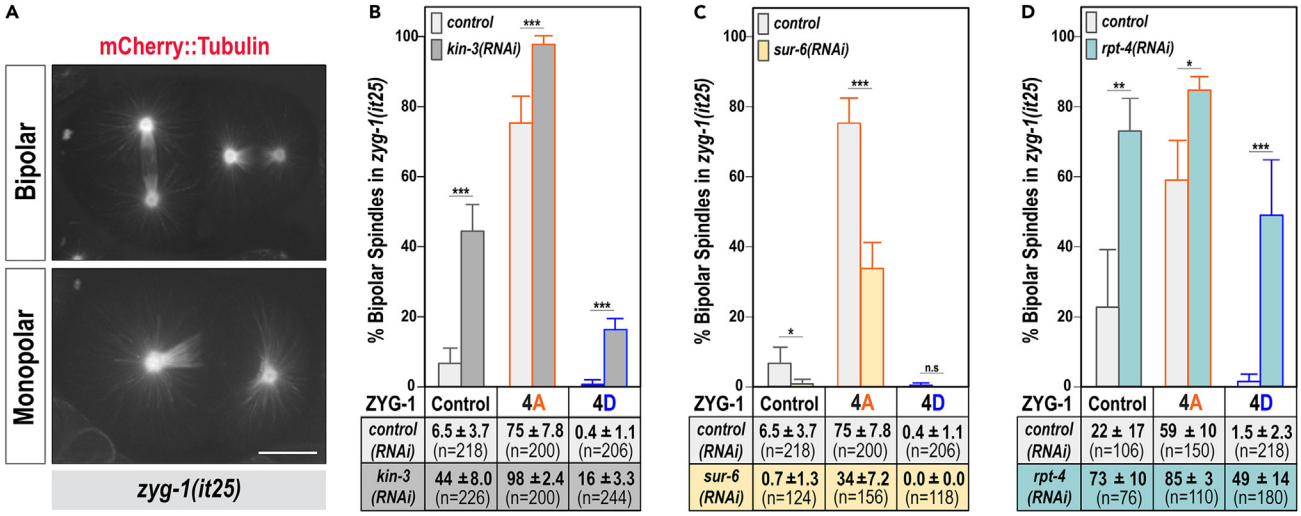

Figure 5. Phosphorylation of ZYG-1 promotes proteasomal degradation of ZYG-1

(A) *zyg-1(it25)* mutant embryos expressing mCherry::Tubulin undergoing second mitosis illustrate bipolar and monopolar spindles. Bar: 10 μm.

(B–D) Quantification of bipolar spindle formation at the second mitosis in *zyg-1(it25)* phospho-mutants at 24°C after knocking down (B) KIN-3, (C) SUR-6, or (D) RPT-4. Data are presented as mean ± SD. n is the number of blastomeres. *$p < 0.05$, **$p < 0.01$, ***$p < 0.001$ (two-tailed unpaired *t* tests).

ZYG-1^{4D} centrosomes (0.73 ± 0.29-fold, $p < 0.001$), compared to controls (1.00 ± 0.40-fold) (Figures 4B and 4C). Similar trends were observed for centrosomal SAS-4, with a significant increase in ZYG-1^{4A} mutants (1.20 ± 0.43-fold, $p < 0.001$) and a decrease in ZYG-1^{4D} mutants (0.73 ± 0.29-fold, $p < 0.001$) (Figures 4B and 4D). We also quantified centrosomal levels of SAS-6, 5, and 4 at the first metaphase, showing similar trends in ZYG-1 phospho-mutants (Figures S4B–S4D).

We next asked how ZYG-1 phosphorylation influences centrosomal levels of SPD-2 that functions upstream of ZYG-1 and is required for centrosomal recruitment of ZYG-1.[14,58] The interaction between SPD-2 and ZYG-1 relies on electrostatic interactions between the N-terminal SPD-2 acidic region and the ZYG-1 CPB basic patch (aa350-560[56]). Since the ZYG-1 L1 domain bridges the kinase and CPB domains, phosphorylation of ZYG-1:4S may affect the interaction between ZYG-1 and SPD-2, influencing centrosomal recruitment of ZYG-1. To assess this, we quantified the total centrosomal signals of SPD-2::2xHA in ZYG-1 phospho-mutants using strains expressing SPD-2::2xHA at the endogenous locus. In contrast to ZYG-1 downstream factors, at the first anaphase, we found no significant changes in total centrosomal SPD-2 levels in ZYG-1^{4A} (1.11 ± 0.58-fold, $p = 0.49$) and ZYG-1^{4D} mutants (1.08 ± 0.56-fold, $p = 0.26$) compared to controls (1.00 ± 0.19-fold, Figure 4E). Likewise, centriolar SPD-2 levels remained unaffected (Figure S4E), and similar trends were observed at the metaphase (Figures S4F and S4G). Furthermore, the phosphorylation state of ZYG-1 did not significantly affect centrosomal levels of the PCM component TBG-1/γ-tubulin during the first mitosis (Figure S4H). Given ZYG-1 acts downstream of SPD-2 in centrosome assembly, our results are consistent with a genetic hierarchy where ZYG-1 phospho-mutations had no significant effect on centrosomal SPD-2.

Collectively, our data illustrate that the phosphorylation state of ZYG-1 affects centrosomal recruitment of downstream centrosome proteins, partially explaining how phosphorylation of ZYG-1 influences centrosome number in the *C. elegans* embryo.

CK2-dependent phosphorylation of ZYG-1

If CK2 targets one or more serine residues in the ZYG-1:4S region (Figure 2A), ZYG-1 phospho-mutants should be less responsive to CK2 depletion than controls. Conversely, if CK2 targets none of the serine residues in this region, ZYG-1 phospho-mutants should be as responsive to CK2 depletion as controls. For the latter, combining CK2 depletion with the ZYG-1^{4A} mutation should show an additive effect. To test this, we used *kin-3(RNAi)* to knockdown KIN-3, the catalytic subunit of CK2, and assayed for bipolar spindle formation in *zyg-1(it25)* genetic backgrounds at the second mitosis (Figures 5A and 5B). As shown in *zyg-1(it25)* controls,[25] *kin-3(RNAi)* significantly increased bipolar spindle formation (44 ± 8%) by 6.7-fold, compared to control RNAi (6.5 ± 3.7%). For ZYG-1^{4A}: *zyg-1(it25)* mutants, control RNAi and *kin-3(RNAi)*-treated embryos produced 75 ± 7.8% and 98 ± 2.4% bipolarity, respectively, showing that *kin-3(RNAi)* only caused a slight (1.3-fold) increase in bipolarity compared to control RNAi. In ZYG-1^{4D}: *zyg-1(it25)* mutants, control RNAi produced nearly zero bipolarity (0.4 ± 1.1%), while *kin-3(RNAi)* led to 16.1 ± 3.3% bipolarity, much lower than expected to be additive (~44%). These results indicate that the PM-ZYG-1^{4D} mutant is partially resistant to CK2 knockdown, further supporting that CK2 phosphorylates one or more serine residues in the ZYG-1:4S region. Additionally, if the ZYG-1:4S region represents the only target sites for CK2 phosphorylation, *kin-3(RNAi)* should not affect % bipolarity in ZYG-1^{4A}: *zyg-1(it25)* mutants. However, *kin-3(RNAi)* led to a moderate but noticeable increase of bipolarity in both *zyg-1(it25)* phospho-mutants (Figure 5B), implying that CK2 likely targets additional ZYG-1 residues or other substrates that influence centrosome assembly directly or indirectly.

PP2A$^{SUR-6/B55}$ May counteract CK2 to balance the phosphorylation state of ZYG-1

In *C. elegans*, the kinase CK2 and the phosphatase PP2A$^{SUR-6/B55}$ play opposing roles in centrosome duplication; CK2 as a negative regulator[25] and PP2A$^{SUR-6/B55}$ as a positive regulator.[30,31] Inhibiting CK2 increases centrosomal ZYG-1 levels,[25] whereas loss of PP2A$^{SUR-6/B55}$ decreases cellular ZYG-1 levels,[31] suggesting that CK2 and PP2A$^{SUR-6/B55}$ counteract to regulate centrosome assembly by controlling ZYG-1 levels. Intriguingly, serine residues in the ZYG-1:4S conform to both CK2 phosphorylation sites[52] and minimal PP2A$^{SUR-6/B55}$ consensus motifs that comprise polybasic residues on each side of the phosphorylation site.[59,60]

Loss of PP2A$^{SUR-6/B55}$ has been shown to enhance monopolar spindles in *zyg-1(it25)* mutants, in contrast to the impact of CK2 depletion.[25,31] A recent study in *C. elegans* also showed that *kin-3* suppresses *sur-6,* encoding the SUR-6/B55 regulatory subunit of PP2A, in centrosome duplication.[61] Our results indicate that the PM-ZYG-1^{4D} mutation enhances monopolar spindles in *zyg-1(it25)* mutants, whereas the NP-ZYG-1^{4A} mutation has the opposite effect (Figure 3B), which led us to speculate that PP2A$^{SUR-6/B55}$ might dephosphorylate the ZYG-1:4S and counteract CK2 to balance the phosphorylation state of ZYG-1. If PP2A$^{SUR-6/B55}$ dephosphorylates serine residues in the ZYG-1:4S region, the phospho-mutants should exhibit partial resistance to SUR-6 inhibition.

We treated animals with *sur-6(RNAi)* to partially deplete PP2A$^{SUR-6/B55}$ and observed centrosome duplication (Figure 5C). Consistent with previous findings,[31] *sur-6(RNAi)* decreased bipolarity in the *zyg-1(it25)* control (0.7 ± 1.3%, 9-fold), compared to control RNAi (6.5 ± 3.7%). In the ZYG-1^{4A}: *zyg-1(it25)* mutants, control RNAi produced 75 ± 7.8% bipolarity, while *sur-6(RNAi)* exhibited 34 ± 7.2% bipolarity. These results suggest partial resistance of the ZYG-1^{4A} to SUR-6 knockdown, supporting that PP2A$^{SUR-6/B55}$ likely targets the ZYG-1:4S region. Moreover, *sur-6(RNAi)* caused a modest yet discernable increase in ZYG-1^{4A}: *zyg-1(it25)* mutants, implying that PP2A$^{SUR-6/B55}$ targets additional ZYG-1 residues or other centrosome proteins, including SAS-5.[30,31] Our collective data suggest that CK2 and PP2A$^{SUR-6/B55}$ target one or more shared serine residues in the ZYG-1:4S region and counteract to balance the phosphorylation state of ZYG-1, providing a regulatory mechanism to ensure that ZYG-1 levels remain above the threshold to support centrosome duplication.

Phosphorylation of ZYG-1 promotes proteasomal degradation

Our data support a model where the phosphorylation state of ZYG-1 regulates overall ZYG-1 levels, likely by influencing protein stability. One possible mechanism is that phosphorylated ZYG-1 in the ZYG-1:4S undergoes proteasomal degradation, while dephosphorylated ZYG-1 is protected from degradation and stabilized. In *C. elegans*, it has been shown that ZYG-1 levels are regulated by the 26S proteasome, partly mediated by the APC/C and SCF E3 ubiquitin ligases.[20] Consistently, *rpt-4(RNAi)*-mediated depletion of RPT-4, an essential subunit of the 26S proteasome, results in elevated ZYG-1 levels at centrosomes,[62] thereby restoring bipolar spindle formation in *zyg-1(it25)* mutants.[20] To test whether ZYG-1 phosphorylation in the ZYG-1:4S promotes proteasomal degradation, we treated ZYG-1 phospho-mutant *zyg-1(it25)* animals with *rpt-4(RNAi)* to partially deplete proteasome activity under conditions that allow completion of meiotic and early mitotic cycles.[31] We then examined how inhibiting the 26S proteasome affected the activity of ZYG-1^{4A} and ZYG-1^{4D} in centrosome duplication (Figure 5D). If *rpt-4(RNAi)* partially blocked degradation of the PM ZYG-1 (ZYG-1^{4D}), *rpt-4(RNAi)* should protect the unstable ZYG-1^{4D} partially from degradation, and then stabilized ZYG-1^{4D} should lead to increased centrosomal ZYG-1 restoring bipolarity in ZYG-1^{4D}: *zyg-1(it25)* embryos.

First, we confirmed that in *zyg-1(it25)* controls, *rpt-4(RNAi)* significantly increased bipolar spindle formation (73 ± 10%) by 3.4-fold, compared to control RNAi (22 ± 17%), consistent with previous work.[20] In ZYG-1^{4A}: *zyg-1(it25)* mutants, *rpt-4(RNAi)* produced a small increase in bipolar spindles (85 ± 3%, 1.4-fold) compared to control RNAi (59 ± 10%). As expected in ZYG-1^{4D}: *zyg-1(it25)* mutants, compared to control RNAi (1.5 ± 2.3%), *rpt-4(RNAi)* produced a stark increase in bipolar spindles (49 ± 14%, 33.5-fold), close to the % bipolarity in the ZYG-1^{4A}: *zyg-1(it25)* mutants (59 ± 10%). Consistently in ZYG-1^{4D} mutants, *rpt-4(RNAi)* led to elevated centrosomal ZYG-1 (1.85 ± 1.60-fold, $p = 0.03$) compared to control RNAi (1.00 ± 0.32-fold) (Figure S4I). These results implicate that ZYG-1^{4D} still retains normal ZYG-1 function, including both the kinase-dependent and kinase-independent roles required for centrosome duplication. Together, *rpt-4(RNAi)* leads to a remarkable stabilization of the ZYG-1^{4D} but a moderate effect on the ZYG-1^{4A}, suggesting that inhibiting the 26S proteasome blocks proteasomal degradation of ZYG-1^{4D}, whereas ZYG-1^{4A} is partially resistant to proteasomal degradation. It seems plausible that phosphorylated ZYG-1 is targeted for proteasomal destruction, triggered by CK2-dependent phosphorylation at ZYG-1:4S. These results support a model where site-specific phosphorylation of ZYG-1 by CK2 regulates ZYG-1 stability through the 26S proteasome, providing a critical mechanism for maintaining the integrity of centrosome number in *C. elegans* embryos.

DISCUSSION

CK2 kinase activity is critical for the integrity of centrosome number

In this study, we demonstrate that inhibiting CK2 leads to centrosome amplification (Figure 1A), highlighting the critical role of CK2 kinase activity in maintaining the proper centrosome number. Since CK2 negatively regulates centrosome duplication by controlling ZYG-1 levels at centrosomes,[25] we hypothesized that CK2 directly phosphorylates ZYG-1 and ZYG-1 phosphorylation by CK2 influences ZYG-1 activity in centrosome assembly. First, we show that CK2 directly phosphorylates kinase-dead ZYG-1 *in vitro,* and physically interacts with ZYG-1 *in vivo* (Figures 1B and 1C). To investigate the functional consequences of ZYG-1 phosphorylation at the putative CK2 target sites, we identified several serine residues in ZYG-1 that conform to the CK2 consensus motif (Table S1). Here, we focused on four serine sites, including S279 and adjacent serine residues (ZYG-1:4S) in the ZYG-1 L1 domain (Figure 2A), which is critical for centrosomal ZYG-1 loading and direct binding to SAS-6,[17,56] and well conserved in closely related nematodes (Figure S2A). Our functional analyses reveal that mutating four serine residues simultaneously produces more potent effects on ZYG-1 activity than the S279 single mutation, indicating that S279 and at least one additional

serine in ZYG-1:4S are phosphorylated *in vivo*. Furthermore, genetic and mass spectrometry analyses suggest that CK2 has at least one target site in ZYG-1:4S *in vivo* (Figure 5B) and phosphorylates at least one serine between S279 and S280 *in vitro* (Figure S2D). These results support the notion that CK2 directly phosphorylates ZYG-1:4S, and phosphorylation of ZYG-1 at multiple sites, including CK2 target sites, regulates ZYG-1 activity in centrosome assembly.

The phosphorylation state of ZYG-1 regulates ZYG-1 stability

Our collective data support that the NP-ZYG-1 mutations mimic loss of CK2. The NP-ZYG-1 mutations restore centrosome duplication and embryonic viability to hypomorphic *zyg-1(it25)* mutants, indicating upregulated ZYG-1 activity. A range of cell division phenotypes (DNA mis-segregation, cytokinesis failure, detached centrosomes, and expanded PCM morphology) observed in NP-ZYG-1^{4A} mutant embryos are closely linked to microtubule-dependent processes. Given the pivotal role of centrosomes as primary microtubule organizing centers, these aberrations could likely arise from abnormal centrosome behavior and its subsequent impact on microtubule organizing capacity. Notably, similar cell division anomalies have been described in several genetic suppressors of *zyg-1*, including CK2[25,27,57] implying a potential link between these observed phenotypes and upregulated ZYG-1 activity. Moreover, a study in human cells[63] highlights that extra centrosomes induced by Plk4 overexpression lead to chromosome missegregation and genomic instability. Remarkably, the NP-ZYG-1 mutations lead to centrosome amplification, reminiscent of the phenotype caused by Plk4/ZYG-1 overexpression. Consistently, total ZYG-1 levels are significantly increased in the NP-ZYG-1 embryos, leading to elevated levels of ZYG-1 and downstream factors at centrosomes, providing a possible mechanism of the NP-ZYG-1 mutation to drive centrosome amplification. Our results suggest that PM-ZYG-1 is stabilized when the 26S proteasome is inhibited, while NP-ZYG-1 is partially resistant to the 26S proteasome. Importantly, the capacity of stabilized PM-ZYG-1 to restore bipolarity highlights that PM-ZYG-1 retains the critical ZYG-1 function for centrosome duplication, including both kinase-dependent and kinase-independent roles. Thus, it seems less likely that our phospho-mutations adversely affect overall ZYG-1 function, including its kinase activity. Rather, these mutations appear to influence ZYG-1 stability. Together, these findings support our model where site-specific phosphorylation of ZYG-1 regulates its stability through proteasomal degradation. Thus, the interplay between CK2 and a phosphatase, potentially PP2A^{B55} based on our analysis discussed in the following text, appears to balance the phosphorylation state of ZYG-1, controlling ZYG-1 levels through proteolysis to limit the centrosome number.

Regulation of CK2-dependent phosphorylation of ZYG-1

Since the kinase CK2 is constitutively active,[64] a refractory mechanism to counteract CK2 should be available for balancing the phosphorylation state of ZYG-1. One mechanism could be through dephosphorylation of ZYG-1 by protein phosphatase. In *C. elegans*, PP2A$^{SUR-6/B55}$ positively regulates ZYG-1 levels,[31] similar to the proposed role of PP2A$^{Twins/B55}$ in stabilizing Plk4 in *Drosophila*.[32] Serine residues in the ZYG-1:4S align with the PP2A^{B55} consensus motif surrounded by polybasic residues[59,60] (Figures 2A, and S2A), suggesting that PP2A$^{SUR-6/B55}$ may stabilize ZYG-1 by counteracting CK2-dependent phosphorylation at ZYG-1:4S. Another possibility is through the substrate availability that restricts ZYG-1 phosphorylation. ZYG-1 undergoes stepwise interactions with centrosome proteins during centrosome biogenesis.[17,56] CK2 target sites in ZYG-1 may be masked or competed by other proteins, preventing CK2 targeting. Such a mechanism has been observed in human cells where Plk4 and CDK-1 compete for binding to STIL/Ana2/SAS-5, providing the temporal regulation of STIL phosphorylation.[65] Alternatively, efficient CK2 targeting may require conformational changes of ZYG-1. In human cells, Plk4 binding to STIL/Ana2/SAS-5 triggers Plk4 kinase activity.[10] Likewise, ZYG-1 binding to another centrosome factor could induce optimal conformation for CK2 targeting. As the ZYG-1:4S resides within the ZYG-1 binding domain to SAS-6,[17] ZYG-1 binding to SAS-6 or another centrosome factor may induce conformational changes of ZYG-1, promoting or blocking CK2 targeting.

Mechanism of ZYG-1 phosphorylation

The mechanism of ZYG-1 phosphorylation in *C. elegans* has been relatively unexplored compared to the extensively studied autophosphorylation of Plk4 in other organisms. Plk4 autophosphorylation in the L1 domain is crucial for its kinase activation and stability,[18,19,23,24,66,67] ensuring proper centrosome number. Our study identifies a cluster of serine residues (ZYG-1:4S) in the ZYG-1 L1 domain that regulates ZYG-1 stability, analogous to Plk4 autophosphorylation. Both Plk4 and ZYG-1 have a conserved SBM responsible for SCF$^{Slimb/\beta TrCP}$-mediated proteolysis.[18–20,23,24] While Plk4 activates the SBM phosphodegron through autophosphorylation,[19,23,24] it remains unclear if ZYG-1 autophosphorylation provides a similar mechanism, although the ZYG-1 SBM plays a conserved role in regulating ZYG-1 stability.[20] The ZYG-1 SBM (aa334-339), located outside ZYG-1:4S (aa273-280), does not conform to the CK2 consensus motif, suggesting that CK2 is unlikely to phosphorylate the ZYG-1 SBM. As ZYG-1 is autophosphorylated *in vitro*,[12] it is tempting to speculate that autophosphorylation of the ZYG-1 SBM promotes SCF-mediated destruction through a conserved mechanism. Therefore, ZYG-1 phosphorylation within ZYG-1:4S may regulate its stability independently of the SCF$^{Slimb/\beta TrCP}$-mediated pathway. In *C. elegans*, centrosomal ZYG-1 levels are regulated by two E3 ubiquitin ligases, the anaphase promoting complex/cyclosome (APC/C)$^{FZR-1}$ and SCF$^{Slimb/\beta TrCP20}$. In humans, Plk4 levels are also regulated by another E3 ubiquitin ligase, Mib1,[68] and TEC tyrosine kinase-dependent phosphorylation,[69] indicating multiple pathways involved in regulating Plk4/ZYG-1 stability. Thus, CK2-dependent phosphorylation of ZYG-1 likely provides an additional regulatory mechanism to fine-tune ZYG-1 activity in centrosome assembly.

Our study provides insights into the mechanism of ZYG-1 phosphorylation and the critical role of CK2 kinase activity in proper centrosome assembly. This study is the first to report that CK2 directly phosphorylates ZYG-1/Plk4 in any organism. Considering the divergence of *C. elegans* ZYG-1 from Plk4 orthologs in other organisms,[70,71] it would be intriguing to investigate whether CK2 also phosphorylates Plk4

orthologs in other species. In human cells, elevated CK2 activity has been observed in cancer cells and normal proliferating cells,[46,47] and dysregulation of CK2α activity has been linked to centrosome amplification. However, the specific targets involved in this process remain unknown.[48] Based on our findings, it is tempting to speculate that CK2 may influence centrosome assembly by phosphorylating Plk4, potentially through a similar regulatory mechanism observed in *C. elegans*. Understanding whether CK2 directly phosphorylates Plk4 and how aberrant CK2 activity relates to abnormal centrosome number in human cells remains important questions for future studies.

Limitations of the study

This study aimed to understand how site-specific phosphorylation of ZYG-1 affects centrosome assembly, focusing on putative CK2-dependent phosphorylation sites. Although we identified a cluster of serine residues that modulate ZYG-1 activity, the exact number of bona fide phosphorylation sites and their individual effects remain unclear. Investigating the impact of individual phosphorylation sites on ZYG-1 activity and centrosome assembly could enhance our understanding of CK2-dependent regulation. Although additional CK2-consensus sites on ZYG-1 were detected, their functional implications were not explored within the scope of this study. Although the potential role of CK2 in regulating Plk4/ZYG-1 levels in humans is intriguing, the lack of sequence homology between Plk4 and ZYG-1 limits our ability to identify corresponding phosphorylation sites on human Plk4.

STAR★METHODS

Detailed methods are provided in the online version of this paper and include the following:

- KEY RESOURCES TABLE
- RESOURCE AVAILABILITY
  - Lead contact
  - Materials availability
  - Data and code availability
- EXPERIMENTAL MODEL AND SUBJECT DETAILS
  - *C. elegans* strains and genetic analysis
- METHOD DETAILS
  - CRISPR/Cas9 genome editing and microinjection
  - Expression and purification of recombinant proteins
  - *In vitro* kinase assays
  - Immunofluorescence and cytological analysis
  - Immunoprecipitation (IP) and western blot
- QUANTIFICATION AND STATISTICAL ANALYSIS

SUPPLEMENTAL INFORMATION

Supplemental information can be found online at https://doi.org/10.1016/j.isci.2023.108410.

ACKNOWLEDGMENTS

This work was supported by a grant (1R15GM147857 to M.H.S.) from the National Institute of General Medical Sciences and Research Excellence Fund (to M.H.S.) from the Center for Biomedical Research at Oakland University. We thank members of the Song lab for experimental assistance and helpful discussion. We thank Kevin O'Connell and Karen Oegema for providing the GST-ZYG-1 expression construct. Some strains were provided by the Caenorhabditis Genetics Center (CGC), which is funded by the Office of Research Infrastructure Programs, National Institutes of Health P40-OD010440.

AUTHOR CONTRIBUTIONS

Conceptualization: J.C.M. and M.H.S.; methodology: J.C.M., C.W., and M.H.S.; validation: M.H.S.; formal analysis: J.C.M., R.N.Y., J.R.D., and M.H.S.; investigation: J.C.M., R.N.Y., J.R.D., B.M. Shaffou, B.M. Sebou, E.C., M. K., and M.H.S.; resources: M.H.S.; data curation: M.H.S.; writing – original draft: M.H.S.; writing – review & editing: J.C.M. and M.H.S.; visualization: M.H.S.; supervision: M.H.S.; project administration: M.H.S.; funding acquisition: M.H.S. All authors read the manuscript.

DECLARATION OF INTERESTS

The authors declare no competing interests.

INCLUSION AND DIVERSITY

We support inclusive, diverse, and equitable conduct of research.

Received: June 12, 2023
Revised: August 21, 2023
Accepted: November 3, 2023
Published: November 8, 2023

REFERENCES

1. Prigent, C., and Uzbekov, R. (2022). Duplication and Segregation of Centrosomes during Cell Division. Cells *11*, 2445.
2. Marthiens, V., and Basto, R. (2020). Centrosomes: The good and the bad for brain development. Biol. Cell *112*, 153–172.
3. Jaiswal, S., and Singh, P. (2021). Centrosome dysfunction in human diseases. Semin. Cell Dev. Biol. *110*, 113–122.
4. Blanco-Ameijeiras, J., Lozano-Fernández, P., and Martí, E. (2022). Centrosome maturation – in tune with the cell cycle. J. Cell Sci. *135*, jcs259395.
5. Ong, J.Y., Bradley, M.C., and Torres, J.Z. (2020). Phospho-regulation of mitotic spindle assembly. Cytoskeleton (Hoboken). *77*, 558–578.
6. Habedanck, R., Stierhof, Y.-D., Wilkinson, C.J., and Nigg, E.A. (2005). The Polo kinase Plk4 functions in centriole duplication. Nat. Cell Biol. *7*, 1140–1146.
7. Ohta, M., Ashikawa, T., Nozaki, Y., Kozuka-Hata, H., Goto, H., Inagaki, M., Oyama, M., and Kitagawa, D. (2014). Direct interaction of Plk4 with STIL ensures formation of a single procentriole per parental centriole. Nat. Commun. *5*, 5267.
8. Dzhindzhev, N.S., Tzolovsky, G., Lipinszki, Z., Schneider, S., Lattao, R., Fu, J., Debski, J., Dadlez, M., and Glover, D.M. (2014). Plk4 Phosphorylates Ana2 to Trigger Sas6 Recruitment and Procentriole Formation. Curr. Biol. *24*, 2526–2532.
9. Kratz, A.-S., Bärenz, F., Richter, K.T., and Hoffmann, I. (2015). Plk4-dependent phosphorylation of STIL is required for centriole duplication. Biol. Open *4*, 370–377.
10. Moyer, T.C., Clutario, K.M., Lambrus, B.G., Daggubati, V., and Holland, A.J. (2015). Binding of STIL to Plk4 activates kinase activity to promote centriole assembly. J. Cell Biol. *209*, 863–878.
11. Moyer, T.C., and Holland, A.J. (2019). PLK4 promotes centriole duplication by phosphorylating STIL to link the procentriole cartwheel to the microtubule wall. Elife *8*, e46054.
12. O'Connell, K.F., Caron, C., Kopish, K.R., Hurd, D.D., Kemphues, K.J., Li, Y., and White, J.G. (2001). The C. elegans *zyg-1* Gene Encodes a Regulator of Centrosome Duplication with Distinct Maternal and Paternal Roles in the Embryo. Cell *105*, 547–558.
13. Woglar, A., Pierron, M., Schneider, F.Z., Jha, K., Busso, C., and Gönczy, P. (2022). Molecular architecture of the *C. elegans* centriole. PLoS Biol. *20*, e3001784.
14. Pelletier, L., O'Toole, E., Schwager, A., Hyman, A.A., and Müller-Reichert, T. (2006). Centriole assembly in *Caenorhabditis elegans*. Nature *444*, 619–623.
15. Delattre, M., Leidel, S., Wani, K., Baumer, K., Bamat, J., Schnabel, H., Feichtinger, R., Schnabel, R., and Gönczy, P. (2004). Centriolar SAS-5 is required for centrosome duplication in *C. elegans*. Nat. Cell Biol. *6*, 656–664.
16. Leidel, S., Delattre, M., Cerutti, L., Baumer, K., and Gönczy, P. (2005). SAS-6 defines a protein family required for centrosome duplication in *C. elegans* and in human cells. Nat. Cell Biol. *7*, 115–125.
17. Lettman, M.M., Wong, Y.L., Viscardi, V., Niessen, S., Chen, S.H., Shiau, A.K., Zhou, H., Desai, A., and Oegema, K. (2013). Direct Binding of SAS-6 to ZYG-1 Recruits SAS-6 to the Mother Centriole for Cartwheel Assembly. Dev. Cell *25*, 284–298.
18. Guderian, G., Westendorf, J., Uldschmid, A., and Nigg, E.A. (2010). Plk4 trans-autophosphorylation regulates centriole number by controlling betaTrCP-mediated degradation. J. Cell Sci. *123*, 2163–2169.
19. Holland, A.J., Lan, W., Niessen, S., Hoover, H., and Cleveland, D.W. (2010). Polo-like kinase 4 kinase activity limits centrosome overduplication by autoregulating its own stability. J. Cell Biol. *188*, 191–198.
20. Medley, J.C., DiPanni, J.R., Schira, L., Shaffou, B.M., Sebou, B.M., and Song, M.H. (2021). APC/CFZR-1 regulates centrosomal ZYG-1 to limit centrosome number. J. Cell Sci. *134*, jcs253088.
21. Rogers, G.C., Rusan, N.M., Roberts, D.M., Peifer, M., and Rogers, S.L. (2009). The SCF Slimb ubiquitin ligase regulates Plk4/Sak levels to block centriole reduplication. J. Cell Biol. *184*, 225–239.
22. Cunha-Ferreira, I., Rodrigues-Martins, A., Bento, I., Riparbelli, M., Zhang, W., Laue, E., Callaini, G., Glover, D.M., and Bettencourt-Dias, M. (2009). The SCF/Slimb Ubiquitin Ligase Limits Centrosome Amplification through Degradation of SAK/PLK4. Curr. Biol. *19*, 43–49.
23. Klebba, J.E., Buster, D.W., Nguyen, A.L., Swatkoski, S., Gucek, M., Rusan, N.M., and Rogers, G.C. (2013). Polo-like Kinase 4 Autodestructs by Generating Its Slimb-Binding Phosphodegron. Curr. Biol. *23*, 2255–2261.
24. Cunha-Ferreira, I., Bento, I., Pimenta-Marques, A., Jana, S.C., Lince-Faria, M., Duarte, P., Borrego-Pinto, J., Gilberto, S., Amado, T., Brito, D., et al. (2013). Regulation of Autophosphorylation Controls PLK4 Self-Destruction and Centriole Number. Curr. Biol. *23*, 2245–2254.
25. Medley, J.C., Kabara, M.M., Stubenvoll, M.D., DeMeyer, L.E., and Song, M.H. (2017). Casein kinase II is required for proper cell division and acts as a negative regulator of centrosome duplication in *Caenorhabditis elegans* embryos. Biol. Open *6*, 17–28.
26. Kemp, C.A., Song, M.H., Addepalli, M.K., Hunter, G., and O'Connell, K. (2007). Suppressors of *zyg-1* Define Regulators of Centrosome Duplication and Nuclear Association in *Caenorhabditis elegans*. Genetics *176*, 95–113.
27. Song, M.H., Aravind, L., Müller-Reichert, T., and O'Connell, K.F. (2008). The Conserved Protein SZY-20 Opposes the Plk4-Related Kinase ZYG-1 to Limit Centrosome Size. Dev. Cell *15*, 901–912.
28. Miller, J.G., Liu, Y., Williams, C.W., Smith, H.E., and O'Connell, K.F. (2016). The E2F-DP1 Transcription Factor Complex Regulates Centriole Duplication in *Caenorhabditis elegans*. G3 (Bethesda). *6*, 709–720.
29. Peel, N., Iyer, J., Naik, A., Dougherty, M.P., Decker, M., and O'Connell, K.F. (2017). Protein Phosphatase 1 Down Regulates ZYG-1 Levels to Limit Centriole Duplication. PLoS Genet. *13*, e1006543.
30. Kitagawa, D., Flückiger, I., Polanowska, J., Keller, D., Reboul, J., and Gönczy, P. (2011). PP2A Phosphatase Acts upon SAS-5 to Ensure Centriole Formation in *C. elegans* Embryos. Dev. Cell *20*, 550–562.
31. Song, M.H., Liu, Y., Anderson, D.E., Jahng, W.J., and O'Connell, K.F. (2011). Protein Phosphatase 2A-SUR-6/B55 Regulates Centriole Duplication in *C. elegans* by Controlling the Levels of Centriole Assembly Factors. Dev. Cell *20*, 563–571.
32. Brownlee, C.W., Klebba, J.E., Buster, D.W., and Rogers, G.C. (2011). The Protein Phosphatase 2A regulatory subunit Twins stabilizes Plk4 to induce centriole amplification. J. Cell Biol. *195*, 231–243.
33. Hu, E., and Rubin, C.S. (1990). Casein kinase II from *Caenorhabditis elegans*. Properties and developmental regulation of the enzyme; cloning and sequence analyses of cDNA and the gene for the catalytic subunit. J. Biol. Chem. *265*, 5072–5080.
34. Hu, E., and Rubin, C.S. (1991). Casein kinase II from *Caenorhabditis elegans*. Cloning, characterization, and developmental regulation of the gene encoding the beta subunit. J. Biol. Chem. *266*, 19796–19802.
35. Wang, X., Gupta, P., Fairbanks, J., and Hansen, D. (2014). Protein kinase CK2 both promotes robust proliferation and inhibits the proliferative fate in the *C. elegans* germ line. Dev. Biol. *392*, 26–41.
36. Park, J.-W., Jeong, J., and Bae, Y.-S. (2022). Protein Kinase CK2 Is Upregulated by Calorie Restriction and Induces Autophagy. Mol. Cell. *45*, 112–121.
37. Huang, J., Wu, Z., Wang, J., and Zhang, X. (2018). Quantitative phosphoproteomics reveals GTBP-1 regulating C.elegans lifespan at different environmental temperatures. Biochem Bioph Res Co *503*, 1962–1967.
38. de Groot, R.E.A., Rappel, S.B., Lorenowicz, M.J., and Korswagen, H.C. (2014). Protein kinase CK2 is required for Wntless internalization and Wnt secretion. Cell. Signal. *26*, 2601–2605.
39. Li, W.-J., Wang, C.-W., Tao, L., Yan, Y.-H., Zhang, M.-J., Liu, Z.-X., Li, Y.-X., Zhao, H.-Q., Li, X.-M., He, X.-D., et al. (2021). Insulin signaling regulates longevity through protein phosphorylation in Caenorhabditis elegans. Nat. Commun. *12*, 4568.
40. Park, J.-H., Lee, J.-H., Park, J.-W., Kim, D.-Y., Hahm, J.-H., Nam, H.G., and Bae, Y.-S. (2017). Downregulation of protein kinase CK2 activity induces age-related biomarkers in C. elegans. Oncotarget *8*, 36950–36963.
41. Hu, J., Bae, Y.-K., Knobel, K.M., and Barr, M.M. (2006). Casein Kinase II and Calcineurin

Modulate TRPP Function and Ciliary Localization. Mol. Biol. Cell *17*, 2200–2211.
42. Alessi, A.F., Khivansara, V., Han, T., Freeberg, M.A., Moresco, J.J., Tu, P.G., Montoye, E., Yates, J.R., Karp, X., and Kim, J.K. (2015). Casein kinase II promotes target silencing by miRISC through direct phosphorylation of the DEAD-box RNA helicase CGH-1. Proc. Natl. Acad. Sci. USA *112*, E7213–E7222.
43. Song, J., and Bae, Y.-S. (2021). CK2 Down-Regulation Increases the Expression of Senescence-Associated Secretory Phenotype Factors through NF-κB Activation. Int. J. Mol. Sci. *22*, 406.
44. Litchfield, D.W. (2003). Protein kinase CK2: structure, regulation and role in cellular decisions of life and death. Biochem. J. *369*, 1–15.
45. Meggio, F., and Pinna, L.A. (2003). One-thousand-and-one substrates of protein kinase CK2? Faseb. J. *17*, 349–368.
46. Firnau, M.-B., and Brieger, A. (2022). CK2 and the Hallmarks of Cancer. Biomed *10*, 1987.
47. Pinna, L.A., and Meggio, F. (1997). Protein kinase CK2 ("casein kinase-2") and its implication in cell division and proliferation. Prog. Cell Cycle Res. *3*, 77–97.
48. St-Denis, N.A., Derksen, D.R., and Litchfield, D.W. (2009). Evidence for regulation of mitotic progression through temporal phosphorylation and dephosphorylation of CK2alpha. Mol. Cell Biol. *29*, 2068–2081.
49. Wolf, B., Balestra, F.R., Spahr, A., and Gönczy, P. (2018). ZYG-1 promotes limited centriole amplification in the *C. elegans* seam lineage. Dev. Biol. *434*, 221–230.
50. Yim, N., Medley, J.C., and Song, M.H. (2022). The *C. elegans* Casein Kinase II is associated with meiotic DNA in fertilized oocytes. Micropublication Biology *2022*, 000583.
51. Salvi, M., Sarno, S., Cesaro, L., Nakamura, H., and Pinna, L.A. (2009). Extraordinary pleiotropy of protein kinase CK2 revealed by weblogo phosphoproteome analysis. Biochim. Biophys. Acta *1793*, 847–859.
52. Schwartz, D., and Gygi, S.P. (2005). An iterative statistical approach to the identification of protein phosphorylation motifs from large-scale data sets. Nat. Biotechnol. *23*, 1391–1398.
53. Ma, R., Li, S., Li, W., Yao, L., Huang, H.-D., and Lee, T.-Y. (2023). KinasePhos 3.0: Redesign and expansion of the prediction on kinase-specific phosphorylation sites. Dev. Reprod. Biol. *21*, 228–241.
54. Wang, C., Xu, H., Lin, S., Deng, W., Zhou, J., Zhang, Y., Shi, Y., Peng, D., and Xue, Y. (2020). GPS 5.0: An Update on the Prediction of Kinase-specific Phosphorylation Sites in Proteins. Dev. Reprod. Biol. *18*, 72–80.
55. Aebersold, R., and Goodlett, D.R. (2001). Mass Spectrometry in Proteomics. Chem. Rev. *101*, 269–295.
56. Shimanovskaya, E., Viscardi, V., Lesigang, J., Lettman, M.M., Qiao, R., Svergun, D.I., Round, A., Oegema, K., and Dong, G. (2014). Structure of the *C. elegans* ZYG-1 Cryptic Polo Box Suggests a Conserved Mechanism for Centriolar Docking of Plk4 Kinases. Structure *22*, 1090–1104.
57. Stubenvoll, M.D., Medley, J.C., Irwin, M., and Song, M.H. (2016). ATX-2, the C. elegans Ortholog of Human Ataxin-2, Regulates Centrosome Size and Microtubule Dynamics. PLoS Genet. *12*, e1006370.
58. Kemp, C.A., Kopish, K.R., Zipperlen, P., Ahringer, J., and O'Connell, K.F. (2004). Centrosome Maturation and Duplication in *C. elegans* Require the Coiled-Coil Protein SPD-2. Dev. Cell *6*, 511–523.
59. Cundell, M.J., Hutter, L.H., Nunes Bastos, R., Poser, E., Holder, J., Mohammed, S., Novak, B., and Barr, F.A. (2016). A PP2A-B55 recognition signal controls substrate dephosphorylation kinetics during mitotic exit. J. Cell Biol. *214*, 539–554.
60. Kruse, T., Gnosa, S.P., Nasa, I., Garvanska, D.H., Hein, J.B., Nguyen, H., Samsøe-Petersen, J., Lopez-Mendez, B., Hertz, E.P.T., Schwarz, J., et al. (2020). Mechanisms of site-specific dephosphorylation and kinase opposition imposed by PP2A regulatory subunits. EMBO J. *39*, e103695.
61. Medley, J.C., and Song, M.H. (2023). *kin-3* genetically suppresses *sur-6* in centrosome assembly during *Caenorhabditis elegans* embryogenesis. Micropublication Biology *2023*, 000791.
62. Peel, N., Dougherty, M., Goeres, J., Liu, Y., and O'Connell, K.F. (2012). The *C. elegans* F-box proteins LIN-23 and SEL-10 antagonize centrosome duplication by regulating ZYG-1 levels. J. Cell Sci. *125*, 3535–3544.
63. Ganem, N.J., Godinho, S.A., and Pellman, D. (2009). A mechanism linking extra centrosomes to chromosomal instability. Nature *460*, 278–282.
64. Turowec, J.P., Duncan, J.S., French, A.C., Gyenis, L., St Denis, N.A., Vilk, G., and Litchfield, D.W. (2010). Protein kinase CK2 is a constitutively active enzyme that promotes cell survival: strategies to identify CK2 substrates and manipulate its activity in mammalian cells. Methods Enzymol. *484*, 471–493.
65. Zitouni, S., Francia, M.E., Leal, F., Montenegro Gouveia, S., Nabais, C., Duarte, P., Gilberto, S., Brito, D., Moyer, T., Kandels-Lewis, S., et al. (2016). CDK1 Prevents Unscheduled PLK4-STIL Complex Assembly in Centriole Biogenesis. Curr. Biol. *26*, 1127–1137.
66. Klebba, J.E., Buster, D.W., McLamarrah, T.A., Rusan, N.M., and Rogers, G.C. (2015). Autoinhibition and relief mechanism for Polo-like kinase 4. Proc. Natl. Acad. Sci. USA *112*, E657–E666.
67. Lopes, C.A.M., Jana, S.C., Cunha-Ferreira, I., Zitouni, S., Bento, I., Duarte, P., Gilberto, S., Freixo, F., Guerrero, A., Francia, M., et al. (2015). PLK4 trans-Autoactivation Controls Centriole Biogenesis in Space. Dev. Cell *35*, 222–235.
68. Čajánek, L., Glatter, T., and Nigg, E.A. (2015). The E3 ubiquitin ligase Mib1 regulates Plk4 and centriole biogenesis. J. Cell Sci. *128*, 1674–1682.
69. Yeung, S.-F., Zhou, Y., Zou, W., Chan, W.-L., and Ching, Y.P. (2022). TEC kinase stabilizes PLK4 to promote liver cancer metastasis. Cancer Lett. *524*, 70–81.
70. Nabais, C., Peneda, C., and Bettencourt-Dias, M. (2020). Evolution of centriole assembly. Curr. Biol. *30*, R494–R502.
71. Carvalho-Santos, Z., Machado, P., Branco, P., Tavares-Cadete, F., Rodrigues-Martins, A., Pereira-Leal, J.B., and Bettencourt-Dias, M. (2010). Stepwise evolution of the centriole-assembly pathway. J. Cell Sci. *123*, 1414–1426.
72. Toya, M., Iida, Y., and Sugimoto, A. (2010). Imaging of mitotic spindle dynamics in *Caenorhabditis elegans* embryos. Methods Cell Biol. *97*, 359–372.
73. Arribere, J.A., Bell, R.T., Fu, B.X.H., Artiles, K.L., Hartman, P.S., and Fire, A.Z. (2014). Efficient marker-free recovery of custom genetic modifications with CRISPR/Cas9 in *Caenorhabditis elegans*. Genetics *198*, 837–846.
74. Dessau, R.B., and Pipper, C.B. (2008). ["R"–project for statistical computing]. Ugeskr Laeger *170*, 328–330.
75. Brenner, S. (1974). The Genetics of *Caenorhabditis elegans*. Genetics *77*, 71–94.
76. Church, D.L., Guan, K.L., and Lambie, E.J. (1995). Three genes of the MAP kinase cascade, *mek-2*, *mpk-1/sur-1* and *let-60* ras, are required for meiotic cell cycle progression in *Caenorhabditis elegans*. Dev Camb Engl *121*, 2525–2535.
77. Kamath, R.S., Fraser, A.G., Dong, Y., Poulin, G., Durbin, R., Gotta, M., Kanapin, A., Le Bot, N., Moreno, S., Sohrmann, M., et al. (2003). Systematic functional analysis of the *Caenorhabditis elegans* genome using RNAi. Nature *421*, 231–237.
78. Paix, A., Folkmann, A., and Seydoux, G. (2017). Precision genome editing using CRISPR-Cas9 and linear repair templates in *C. elegans*. Methods *121–122*, 86–93.
79. Paix, A., Folkmann, A., Rasoloson, D., and Seydoux, G. (2015). High Efficiency, Homology-Directed Genome Editing in *Caenorhabditis elegans* Using CRISPR-Cas9 Ribonucleoprotein Complexes. Genetics *201*, 47–54.
80. Safran, A., Neumann, D., and Fuchs, S. (1986). Analysis of acetylcholine receptor phosphorylation sites using antibodies to synthetic peptides and monoclonal antibodies. EMBO J. *5*, 3175–3178.

STAR★METHODS

KEY RESOURCES TABLE

REAGENT or RESOURCE	SOURCE	IDENTIFIER
Antibodies		
DM1a	Sigma	T9026
α-Myc	ThermoFisher	PA1-981
α-Myc	Genscript	A00704
α-V5	MBL	M167-3
α-V5	Genscript	A01724
α-HA	ThermoFisher	26183
α-GFP	Roche	11814460001
α-Ollas	ThermoFisher	MA5-16125
α-ZYG-1	Stubenvoll et al.[57]	N/A
α-SAS-4	Song et al.[27]	N/A
α-SAS-5	Medley et al.[25]	N/A
α-SAS-6	Song et al.[31]	N/A
α-Myc Magnetic Beads	MBL	M047-11
Goat α-Mouse IgG AlexaFluor 488	ThermoFisher	A11001
Goat α-Mouse IgG AlexaFluor 568	ThermoFisher	A11004
Goat α-Rat IgG AlexaFluor 488	ThermoFisher	A11006
Goat α-Rabbit IgG AlexaFluor 488	ThermoFisher	A11034
Goat α-Rabbit IgG AlexaFluor 568	ThermoFisher	A11036
IRDye 680RD Donkey α-Guinea Pig IgG	LICOR	926-68077
IRDye 680RD Donkey α-Mouse IgG	LICOR	926-68072
IRDye 680RD Donkey α-Rabbit IgG	LICOR	926-68073
IRDye 680RD Goat α-Rat IgG	LICOR	926-68076
IRDye 800CW Donkey α-Mouse IgG	LICOR	926-32212
IRDye 800CW Donkey α-Rabbit IgG	LICOR	926-32213
Bacterial and virus strains		
Escherichia coli OP50	CGC	OP50
Escherichia coli NA22	CGC	NA22
Escherichia coli HT115	CGC	HT115(DE3)
Escherichia coli HT115: L4440	Addgene	L4440
Escherichia coli HT115: *kin-3(RNAi)*	*C. elegans* ORFeome	*kin-3(RNAi)*
Escherichia coli HT115: *sur-6(RNAi)*	Ahringer RNAi Library	*sur-6(RNAi)*
Escherichia coli HT115: *rpt-4(RNAi)*	Ahringer RNAi Library	*rpt-4(RNAi)*
Escherichia coli Rosetta 2(DE3) pLysS	Sigma (Novagen)	70956-3
Chemicals, peptides, and recombinant proteins		
Alt-R S.p. Cas9 Nuclease V3	IDT	1081058
ZYG-1^{4S} Peptide: RRQRSREPVRSSRDDRSRDGR	Genscript	ZYG-1:WT
ZYG-1^{4A} Peptide: RRQRAREPVRAARDDRARDGR	Genscript	ZYG-1:4A
ZYG-1^{S279A} Peptide: RRQRSREPVRASRDDRSRDGR	Genscript	ZYG-1:S279A
ZYG-1^{S280A} Peptide: RRQRSREPVRSARDDRSRDGR	Genscript	ZYG-1:S280A
Recombinant Human CK2	NEB	P6010S

(*Continued on next page*)

Continued

REAGENT or RESOURCE	SOURCE	IDENTIFIER
Recombinant Human PKA	NEB	P6000S
PreScission Protease	GenScript	Z02799
4,5,6,7-tetrabromobenzotriazole (TBB)	Tocris	2275
MG132	Tocris	1748
cOmplete Protease Inhibitor	Sigma (Roche)	11697498001
Experimental models: Organisms/strains		
C. elegans: Strain N2 *wild type*	CGC	N2
C. elegans: Strain OC14 *zyg-1(it25[ZYG-1^{P442L}]) II*	O'Connell et al.[12]	OC14
[a]*C. elegans*: Strain MTU21 *zyg-1(mhs389it25[ZYG-1$^{4D:P442L}$]) II*	This Study	MTU21
C. elegans: Strain MTU25 *zyg-1(mhs399it25[ZYG-1$^{S279A:P442L}$]) II*	This Study	MTU25
C. elegans: Strain MTU44 *zyg-1(mhs404it25[ZYG-1$^{S279D:P442L}$]) II*	This Study	MTU44
[a]*C. elegans*: Strain MTU50 *zyg-1(mhs409[ZYG-1^{4D}]) II*	This Study	MTU50
[b]*C. elegans*: Strain MTU86 *zyg-1(mhs428it25[ZYG-1$^{4A:P442L}$]) II*	This Study	MTU86
[b]*C. elegans*: Strain MTU127 *zyg-1(mhs454[ZYG-1^{4A}]) II*	This Study	MTU127
C. elegans: Strain MTU137 *kin-3(mhs464[KIN-3::V5] I*	Yim et al.[50]	MTU137
C. elegans: Strain MTU150 *sas-6(mhs451[Ollas::SAS-6]) IV*	Medley et al.[20]	MTU150
C. elegans: Strain MTU158 *zyg-1(mhs454) II; sas-6(mhs451) IV*	This Study	MTU158
C. elegans: Strain MTU159 *zyg-1(mhs409) II; sas-6(mhs451) IV*	This Study	MTU159
[a]*C. elegans*: Strain MTU178 *zyg-1(mhs456mhs482[2xMyc::ZYG-1^{4D}]) II*	This Study	MTU178
[b]*C. elegans*: Strain MTU209 *zyg-1(mhs507mhs454[2xMyc::ZYG-1^{4A}]) II*	This Study	MTU209
C. elegans: Strain MTU257 *sas-5(mhs533[SAS-5::V5]) V*	Medley et al.[20]	MTU257
C. elegans: Strain MTU271 *zyg-1(mhs456[2xMyc::ZYG-1]) II*	Medley et al.[20]	MTU271
C. elegans: Strain MTU299 *zyg-1(mhs507mhs454) II; unc-119(ed3) III; bsIs15[pNP99:unc-119(+) tbb1p::mCherry::tbb-2::tbb-2 3'UTR*	This Study	MTU299
C. elegans: Strain MTU337 *spd-2(mhs580[SPD-2::2xHA]) I*	This Study	MTU337
C. elegans: Strain MTU371 *zyg-1(mhs454) II; sas-5(mhs533) V*	This Study	MTU371
C. elegans: Strain MTU373 *zyg-1(mhs409) II; sas-5(mhs533) V*	This Study	MTU373
C. elegans: Strain MTU376 *spd-2(mhs580) I; zyg-1(mhs454) II*	This Study	MTU376
C. elegans: Strain MTU377 *spd-2(mhs580) I; zyg-1(mhs409) II*	This Study	MTU377
C. elegans: Strain MTU746 *zyg-1(mhs456) II; unc-119(ed3) III; bsIs15[pNP99:unc-119(+) tbb1p::mCherry::tbb-2::tbb-2 3'UTR*	This Study	MTU746
C. elegans: Strain MTU806 *kin-3(mhs464) I; zyg-1(mhs456) II*	This Study	MTU806
C. elegans: Strain OC481 *unc-119(ed3) III; bsIs15[pNP99: unc-119(+) tbb-1p::mCherry::tbb-2::tbb-2 3'UTR*	Medley et al.[25]	OC481
C. elegans: Strain SA250 *jIs54[pie-1p::GFP::tbb-2 + pie-1p:: 2xmCherry::tbg-1 + unc-119(+)]; tjIs57[pie1p::mCherry::his-48 + unc119(+)]*	Toya et al.[72]	SA250
[a]ZYG-1^{4D}: S273D,S279D,S280D,S285D [b]ZYG-1^{4A}: S273A,S279A,S280A,S285A		
Oligonucleotides		
crRNA Targeting *dpy-10* for co-CRISPR: UUCUGCUGUCUUGAUUGACG	Arribere et al.[73]	N/A
crRNA Targeting *spd-2* C-terminus: UCUAUUCGAAAAUCUUGUAU	This Study	N/A
crRNA Targeting *zyg-1* N-terminus: UUGAUCAACUAUGAGAUGAG	Medley et al.[20]	N/A
crRNA Targeting *zyg-1* L1 domain: UGGACGACGACAGAGAUCGA	This Study	N/A
Repair Template for *dpy-10* co-conversion: CACTTGAACTTCAATACG GCAAGATGAGAATGACTGGAAACCGTACCGCATGCGGTGCCTA TGGTAGCGGAGCTTC ACATGGCTTCAGACCAACAGCCTAT	Arribere et al.[73]	N/A

(*Continued on next page*)

Continued

REAGENT or RESOURCE	SOURCE	IDENTIFIER
Repair Template for SPD-2::2xHA: AATCAGACATTTGTCAACGACG TTACAATTGTTCCGAATACAAGATTTTCGAATAGAAAGGGAGGTT CCGGTGGATCTGGTGGATCCTACCCATACGATGTTCCAGATT ACGCTTATCCATATGATGTTCCAGATTATGCTTAAAATCTTAACCTA ACTTTCCAAATATTCTCTG	This Study	N/A
Repair Template for 2xmyc::ZYG-1: ATACGCTGTGCGAACGT ATGAGAAAACTACATCAAGGTGGAAGTGGTGGCTCGGGT GGCTCTTACCCTTATGACGTACCAGATTACGCGTATCCAT ACGATGTCCCTGATTACGCATAATAGTAATAACTTAGTAT ACGATGAGTTTTGCTCTTACTTCATGTGCTCCTACATTTT ACCACATA	Medley et al.[20]	N/A
Repair Template for ZYG-1^{S279A}: AGAACACTCGCGGGATGGA CGACGACAGAGATCGCGAGAACCAGTAAGAGCCTCAA GAGATGATCGATCTCGAGA TGGCAGAGCTCT	This Study	N/A
Repair Template for ZYG-1$^{4A[S273A,S279A,S280A,S285A]}$: CTTCTCGAGAGAACA CTCGCGGGATGGACGACGACAGAGAGCCAGAGAACCAGTACGT GCCGCCAGAGATGATCGAGCCCGAGATGGCAGAGCTCTGAT AAGGTCTTCGAGTCAACCTGC	This Study	N/A
Repair Template for ZYG-1^{S279D}: AGAACACTCGCGGGATGG ACGACGACAGAGATCGCGAGAACCAGTAAGAGACTCAA GAGATGATCGATCTCGAGATGGCAGAGCTCT	This Study	N/A
Repair Template for ZYG-1$^{4D[S273D,S279D,S280D,S285D]}$: CTTCTCGAGAGAAC ACTCGCGGGATGGACGACGACAGAGAGACAGAGAACCAGTACGTGA CGACAGAGATGATCGAGATCGAGATGGCAGAGCTCTGATAA GGTCTTCGAGTC AACCTGC	This Study	N/A
Recombinant DNA		
Plasmid for Expressing Full Length ZYG-1	Lettman et al.[17]	pMB01
Plasmid for Expressing Full Length Kinase Dead ZYG-1	Genscript	pGEX-6P-1
Software and algorithms		
Adobe Illustrator	Adobe	RRID:SCR_010279
Adobe Photoshop	Adobe	RRID:SCR_014199
GPS 5.0	Wang et al.[54]	RRID:SCR_016374
Kinase Phos3.0	Ma et al.[53]	RRID:SCR_023595
R	Dessau et al.[74]	RRID:SCR_001905

RESOURCE AVAILABILITY

Lead contact

Inquiries and requests for resources should be directed to and will be fulfilled by the lead contact, Dr. Mi Hye Song (msong2@oakland.edu).

Materials availability

All unique reagents generated in this study are available from the lead contact with a completed Materials Transfer Agreement.

Data and code availability

- All data reported in this paper will be shared by the lead contact upon request.
- This study does not report original code.
- Any additional information required to reanalyze the data reported in this paper is available from the lead contact upon request

EXPERIMENTAL MODEL AND SUBJECT DETAILS

C. elegans strains and genetic analysis

All strains used in this study were derived from the N2 wild-type strain.[75,76] Animals were maintained at 16 or 19°C on MYOB plates seeded with *Escherichia coli* OP50. For embryonic lethality assays, L4 animals were transferred to individual plates and allowed to produce progeny for 24–48 h. Progeny was then allowed to develop for 18–24 h before scoring the number of larva and unhatched (dead) embryos. RNAi feeding was performed as previously described[77] using the L4440 empty vector as a negative control. Partial depletion of *rpt-4* was achieved by briefly feeding for 12–18 h before imaging. A complete list of *C. elegans* strains used in this study is provided in Table S3.

METHOD DETAILS

CRISPR/Cas9 genome editing and microinjection

Microinjection was performed using the XenoWorks microinjector (Sutter Instruments, Novato, CA) with a continuous pulse setting at 400–800 hPa. For all genome editing, we used the *dpy-10(cn64)* co-CRISPR technique as previously described.[73,78] Animals were microinjected with Cas9 RNP complexes preloaded with equimolar crRNA (0.4–0.8 μg/μl each) and tracrRNA molecules (12 μg/μl) as previously described.[79] Single-stranded oligonucleotide repair templates were included at 25–100 ng/μl. Cas9 and custom-designed oligonucleotides (Tables S4 and S5) were purchased from IDT (Coralville, IA). Following injection, F1 generation *dpy-10(cn64)* II/+ rollers were screened for each co-edit. All genotypes were verified in homozygous F2 generation animals through Sanger Sequencing (GeneWiz, South Plainfield, NJ).

Expression and purification of recombinant proteins

pGEX-6P-1 plasmids for expressing full length ZYG-1 were provided by Genewiz and transformed into Rosetta 2(DE3) pLysS cells. Starter cultures were inoculated using 2L of LB media and grown at 37°C until the mixture reached an optical density of 0.4–0.6 at 600 nm. Protein expression was induced by adding 1 mM isopropyl ß-D-1-thiogalactopyranoside (IPTG) and incubating the cultures overnight at 16°C (250 rpm). The cells were harvested by centrifugation at 4,000 rcf, and the pellet was resuspended in Lysis Buffer [PBS with 250mM NaCl, 10mM EDTA, 0.1% Tween 20, 200 μg/ml Lysozyme, 0.1% PMSF]. The cells were lysed by sonication at 40% amplitude and a 10s/50s on/off pulse using a 505 Sonic Dismembrator equipped with a ¼" titanium probe (Fisher Scientific). The lysate was then clarified by centrifugation at 18,500 rpm for 1.5 hours using a Sorvall RC5C Plus centrifuge equipped with a SS34 rotor. The supernatant was then applied to a 10 mL packed GST resin (GE Healthcare, Waukesha, WI) equilibrated in Wash Buffer [PBS with 250 mM NaCl and 1 mM DTT]. The column was washed with 3x 20mL volumes of Wash Buffer, and the GST fusion proteins were eluted in 50 mM Tris [pH 8.1], 150 mM KCl, and 1mM DTT through a 5–50 mM glutathione gradient. The protein elutions were identified by SDS-PAGE and A280 absorbance, and the samples were dialyzed against Storage Buffer [20mM HEPES pH 7.5, 150mM KCl, 1mM DTT, and 40% Glycerol]. After three exchanges (4 hours each), the concentrated protein samples were snap-frozen in liquid nitrogen and stored at −80°C until use.

In vitro kinase assays

Recombinant human Casein Kinase 2 (NEB, P6010S) and Protein Kinase A (NEB, P6000S) were purchased from New England Biolabs. Recombinant GST::ZYG-1^{K41M} (kinase-dead)[12,17] fusion proteins were expressed in *Escherichia coli* and purified using glutathione resin. Protein concentration was determined using a nanodrop spectrophotometer. For kinase reactions using full-length ZYG-1, 1 μg of recombinant ZYG-1 proteins were incubated with 1 μg of recombinant CK2 in kinase buffer [500 mM Tris-Cl, 100 mM $MgCl_2$, 1 mM EDTA and 20 mM DTT] in a final volume of 10 μL for 30 minutes at room temperature. Following kinase reactions, proteins were analyzed by SDS/PAGE and autoradiography. ZYG-1 peptides were produced by Genscript (Piscataway, NJ). For ZYG-1 peptide analysis, 5–10 μg of ZYG-1 peptides were incubated at room temperature for 30 minutes with 1 μg of recombinant CK2 in kinase buffer [500 mM Tris-Cl, 100 mM $MgCl_2$, 1 mM EDTA and 20 mM DTT] in a final volume of 10 μL. Peptides were then analyzed through thin layer chromatography and autoradiography as previously described.[80] In brief, the phosphorylated peptides were loaded on silica plates and allowed to chromatograph for 4 h at room temperature. A mixture of n-butanol, acetic acid, pyridine, and water (3:1:2:4 ratio) was used as a solvent. For all *in vitro* kinase reactions, 200 μM of cold ATP and 4 μCi of ATP[γ-^{32}P] were included in each reaction. To inhibit CK2 activity, 5 μM TBB (4,5,6,7-tetrabromobenzotriazole, Tocris, 2275) was added to reactions. For mass spectrometry, ZYG-1 peptides following *in vitro* kinase reaction without γ-^{32}P were analyzed for the phosphorylation events by the Taplin Mass Spectrometry facility as described previously.[31]

Immunofluorescence and cytological analysis

Confocal microscopy was performed as previously described,[27] using a Nikon Eclipse Ti-U microscope equipped with a Plan Apo 60 × 0.4 NA lens, a Spinning Disk Confocal (Yokogawa, CSU-X1), and a Photometrics Evolve 512 camera. The following primary antibodies were used at 1:3000 dilutions: DM1a (Sigma, T9026), α-ZYG-1,[57] α-SAS-4,[27] α-Myc (ThermoFisher, PA1-981), α-V5 (MBL, M167-3), α-HA (ThermoFisher, 26183) and α-Ollas (ThermoFisher, MA5-16125). Alexa Fluor 488 and 568 secondary antibodies (ThermoFisher, A11001, A11004, A11006, A11034, A11036) were used at 1:3000 dilutions.

Image acquisition and quantification of fluorescence intensity were performed using MetaMorph software (Molecular Devices, Sunnyvale, CA, USA). Adobe Creative Cloud 2023 (Photoshop/Illustrator) was used for image processing. To quantify centriolar signals, the average intensity within 8 or 9-pixel (1 pixel = 0.151 μm) diameter region was recorded for a single focal plane within an area centered on the centrosome. To measure total centrosomal (both centriolar and PCM-associated) SPD-2 levels and centrosomal TBG-1 levels, the average intensity

within a 20-pixel diameter region was recorded for a single focal plane centered on the centrosome. For background subtraction, the average intensity within a 25-pixel diameter region drawn outside the embryo was used.

Samples were prepared following a uniform protocol across all experimental and control groups. Slides were prepared and scanned in alternating order to minimize experimental variations. Images were acquired under consistent conditions, including identical microscope settings and exposure times. For quantification, consistent cell cycle staging was always used. Normalization was done relative to controls and on a per-experiment basis. At least five experimental replicates were performed for each set of quantification. Each experimental replicate was normalized to their respective controls. All slides from one replicate were scanned in a single session. Personnel involved in quantification remained blinded to sample identities to minimize potential biases.

Immunoprecipitation (IP) and western blot

IP experiments were performed as described.[57] Embryos were extracted from adult worms using hypochlorite treatment (1:2:1 ratio of M9 buffer, 5.25% sodium hypochlorite, and 5 M NaOH), washed five times using M9 buffer, frozen in liquid nitrogen and stored at −80°C until use. Embryos were suspended in lysis buffer [50 mM HEPES, pH 7.4, 1 mM EDTA, 1 mM $MgCl_2$, 200 mM KCl, and 10% glycerol (v/v)] supplemented with complete protease inhibitor cocktail (Roche, Basel, Switzerland) and MG132 (Tocris, Avonmouth, Bristol, UK). Embryos were then milled for 5 minutes (repeat x3) at 30 Hz using a Retsch MM 400 mixer-mill (Verder Scientific, Newtown, PA) and sonicated for 3 minutes in an ultrasonic water bath (Thermo Fisher, Waltham, MA).

Lysates were spun at 45,000 rpm for 45 minutes using a Sorvall RC M120EX ultracentrifuge (Thermo Fisher), then the supernatant was recovered to clean tubes. Protein concentrations were determined using a nanodrop spectrophotometer, and the equivalent amount of total protein lysates was used for IP. Embryonic protein lysates mixed with α-Myc magnetic beads (MBL, M047-11) were incubated by rotation for 1 hour at 4°C and washed (3 × 5 minutes) with PBST (PBS + 0.1% Triton-X 100). IP with beads and input samples were resuspended in 2X Laemmli Sample Buffer (Sigma) and boiled for 5 minutes before fractionating on a 4–12% NuPAGE Bis-Tris gel (Invitrogen) and transferred to nitrocellulose membrane. The following antibodies were used at 1:3000-10,000 dilutions: DM1a (Sigma, T9026), α-V5 (Genscript, A01724), α-Myc (Genscript, A00704), α-SAS-6,[31] and IRDye secondary antibodies (LI-COR Biosciences). Blots were imaged using the Odyssey infrared scanner (LI-COR Biosciences) and analyzed using Image Studio software (LI-COR Biosciences).

QUANTIFICATION AND STATISTICAL ANALYSIS

Statistics were generated using R statistical software and presented as mean ± standard deviation (s.d.). Dotplots were generated using the R 'beeswarm' package. In the dotplots, boxes range from the first through third quartile of the data. Thick bar indicates the median. Solid gray line extends 1.5 times the inter-quartile range or to the minimum and maximum data point. All p values were calculated using two-tailed t-tests: $^{ns}p > 0.05$; $*p < 0.05$; $**p < 0.01$; $***p < 0.001$.